STUDIA

UNIVERSITATIS BABEŞ-BOLYAI

PHYSICA

2

1986

CLUJ-NAPOCA

ANUL XXXI 1986

STUDIA

UNIVERSITATIS BABEŞ-BOLYAI

PHYSICA

2

Redacţia 3400 CLUJ-NAPOCA, str. M Kogălniceanu, 1 Telefon ● 1 61 01

SUMAR — CONTENTS

STUDIA UNIV BABEŞ—BOLYAI, PHYSICA, XXXI, 2, 1986

MICROSCOPIC THEORY OF THE LOWER CRITICAL FIELD OF SUPERCONDUCTING ALLOYS

M. CRIŞAN* and T. VERES*

Received February 2, 1986

ABSTRACT. — The BCS model for a superconductor has been used for lower critical field H_{c1} of superconducting alloys The method can be generalized for antiferromagnetic and the spin-glass superconductors

Introduction. The lower critical field H_{c1} is one of the most important parameters for type—II superconductors, but until now its temperature dependence has been calculated using the phenomenological theory given by Abrikosov [1]

The purpose of this paper is to give a general method for calculating the criticla field H_{c1} for superconducting alloys using the microscopic model in the version of the Gor'kov equations The superconducting alloy is considered as a type—II superconductor in the mixed state, containing a finite number of vortices The flux and the currents associated with an isolated vortex line are extended over a distance $\lambda_L(\lambda_L$ — the London penetration depth) The region over which the order parameter $\Delta(r)$ varies from zero to its full value Δ is called core of the vortex Caroli *et al* [2] have shown that the core of the vortex line contains low-lying energy levels for single electrons, rather like in a normal metal. Futher on, this justifies treatment of the core as a normal region. The existence of these quasi-normal excitations in the core has been confirmed by many experimental results

Recently, the theory on mixed state magnetic superconductors has been reconsidered by Tachiki *et al.* [3] and Matsumoto *et al* [4], using a semiphenomenological theory The most important result obtained in [3—4] is the possibility of a new transition near T_m (T_m is the critical magnetic temperature) from a type—II superconductor to a type—I The calculation of the lower critical field H_{c1} in this case has been performed by usual thermodynamics.

In Section II we will show how the thermodynamic potential can be calculated using the Gor'kov equations, which will be solved in Section III in an approximation imposed by the calculation of H_{c1}. In Section IV we show that this general method can be applied for antiferromagnetic superconductors and for spin-glass superconductors.

The general Method for Calculation of the Lower Critical Field The temperature dependence of H_{c1} has been measured for superconducting materials, but it has been calculated through phenomenological theory.

* *University of Cluj-Napoca, Department of Physics, 3400 Cluj-Napoca, Romania*

The aim of this paper is to show that H_{c1} can be calculated using the microscopic model and the method of Gor'kov equations We will proceed with the simple thermodynamical consideration concerning the mixed state.

If we denote by E_1 the energy of one vortex, the mixed state becomes unstable at

$$H_{c1} = \frac{4\pi}{\Phi_0} E_1 \tag{1}$$

where $\Phi_0 = hc/2e$ is the flux quantum, and E_1 is the energy of one vortex which is well approximated by a normal cylinder of radius (coherence length) within which order parameter $\Delta(\vec{r})$ vanishes, and beyond which it has its full value denoted by Δ The region where $\Delta(r)$ varies from zero to its full value is called the core of the vortex and the energy of the vortex is in fact

$$E_1 = E_v + E_c$$

where

$$E_c = \frac{\Phi_0^2}{32\pi^2\lambda_L^2}$$

and E_v will be calculated from the microscopic model.
This energy can be defined as

$$E_v = F_n(\Delta) - F_0(\Delta) = \int d^3\vec{r} \int_0^g \frac{\Delta^2(\vec{r}) - \Delta}{\Delta} d\left(\frac{1}{g}\right) \tag{2}$$

where g is the coupling constant from the self-consistent equation for the gap, and is given by

$$\frac{1}{g} = \frac{\pi T}{(2\pi)^3} \sum_n \int d^3\vec{p} \frac{1}{\omega^2 + \varepsilon^2(p) + \Delta^2} \tag{3}$$

with $\omega = \pi T\left(n + \frac{1}{2}\right)$.
From Equation (3) we get

$$d\left(\frac{1}{g}\right) = A(\Delta)\frac{d\Delta}{\Delta}\,; \quad A(\Delta) = \frac{-mp_0}{2\pi} \Delta^2 \pi T \sum_n \frac{1}{E^3} \tag{4}$$

where

$$E^2 = \omega^2 + \Delta^2. \tag{5}$$

From Equation (2) we obtain the vortex energy E_v as

$$E_v = 2\pi \int_0^\Delta d\Delta \int_0^\infty r dr \frac{\Delta^2(r) - \Delta^2}{\Delta} A(\Delta) \tag{6}$$

and if we use

$$\Delta(\vec{r}) = \Delta + \Delta_1(\vec{r}) + \dots$$

$$\Delta^2(\vec{r}) - \Delta^2 \cong 2\Delta(\Delta(\vec{r}) - \Delta) \tag{7}$$

Equation (6) becomes

$$E_v = 4\pi \int_0^{\Delta} d\Delta \int_0^{\infty} r dr \Delta_1(r) A(\Delta) \tag{8}$$

where correction $\Delta_1(\vec{r})$ in the order parameter is due to the presence of the magnetic field Using this approximation we will take the important contribution between λ_L/k and λ_L (λ_L is the London penetration depth, k(T) Ginzburg—Landau parameter) neglecting the contribution from λ_L to ∞ including in E_c the contribution of the normal part.

In the next paragraph we will calculate E_v from the Gor'kov equations

The Gor'kov Equations The superconductor in an electromagnetic field described by a potential vector $\vec{A}(\vec{r})$ can be studied using the equations

$$\hat{O}(\Delta\,,\ A(\vec{r}))\hat{G}(\vec{r},\ \vec{r}'\,,\ \omega) = \hat{1}\delta(\vec{r} - \vec{r}') \tag{9}$$

where

$$\hat{O} = \begin{bmatrix} i\omega + \frac{1}{2m}(\Delta - ieA(r)^2 + \mu\,,\ \Delta(\vec{r}) \\ -\Delta(r)\,,\ -i\omega + \frac{1}{2m}(\Delta + ieA(r))^2 + \mu \end{bmatrix} \tag{10}$$

and the Green function

$$\begin{bmatrix} G(\vec{r},\ \vec{r}'\,,\ \omega)\,; & -F(\vec{r},\ \vec{r}'\,,\ \omega) \\ F^+(\vec{r},\ \vec{r};\ \omega); & G(\vec{r},\ \vec{r};\ -\omega) \end{bmatrix} \tag{11}$$

with

$$G^+(\vec{r},\ \vec{r}'\,,\ \omega) = G(\vec{r},\ \vec{r}'\,,\ -\omega)$$

$$F(\vec{r},\ \vec{r}'\,,\ \omega) = F(\vec{r},\ \vec{r}',\ -\omega)$$

The order parameter defined as

$$\Delta(r) = g\pi T \sum_n F(\vec{r},\ \vec{r}'\,,\ \omega)$$

can be obtained from a self-consistent equation written under the from of (3) The solution of Equation (9) can be obtained by a general method given by Jacobs [5] as a series

$$\hat{G}^{(n)}(\vec{r}, \vec{r}', \omega) = -\int d^3\vec{r}_1 \hat{G}^0(\vec{r}, \vec{r}_3, \omega) \sum_{m=0}^{\infty} \hat{O}_{n-m}(\vec{r}_3) \hat{G}^{(m)}(\vec{r}_3 \vec{r}, \omega) \tag{12}$$

where $\hat{G}_0$ is the Green function for $\vec{A} = 0$

Using this general result we have

$$G(\vec{r}, \vec{r}', \omega) = \hat{G}^0(\vec{r}, \vec{r}', \omega) + \frac{ie}{m} \int d^3\vec{r}_3 \hat{G}^0(\vec{r}, \vec{r}_3, \omega) \left(\vec{A}(r_3) \frac{\partial}{\partial r_3}\right) \hat{G}(\vec{r}_3, \vec{r}, \omega) -$$

$$- \int d^3\vec{r}_3 \hat{G}^0(\vec{r}, \vec{r}_3, \omega) \Delta_1(\vec{r}_3) \hat{G}(\vec{r}_3, \vec{r}, \omega) \tag{13}$$

where $\Delta_1(r)$ has been defined in (7)

This equation contains only the linear terms in $A(\vec{r})$, but in order to calculate the correction $\Delta_1(r)$ we have to consider the second order correction in which it will be proportional to $A^2(r)$ The linear terms in $A(\vec{r})$ do not appear in $\Delta_1(r)$ because $\operatorname{div} \vec{A}(\vec{r}) = 0$

The Fourier transform of (13) contains the first order corrections given by the diagrams

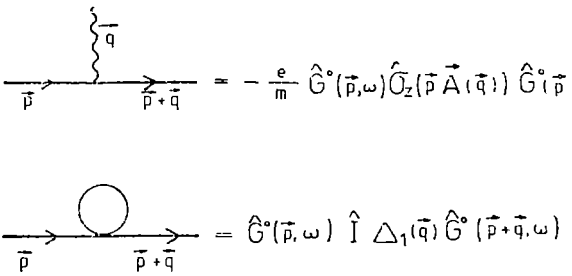

Fig 1

where

$$\hat{\sigma}_z = \begin{pmatrix} 1, & 0 \\ 0, & -1 \end{pmatrix} \quad \hat{I} = \begin{pmatrix} 0, & -1 \\ 1, & 0 \end{pmatrix}$$

and $\Delta_1(q) = \Delta(q) - \Delta$

The second order correction in the Green function will be given by the diagram

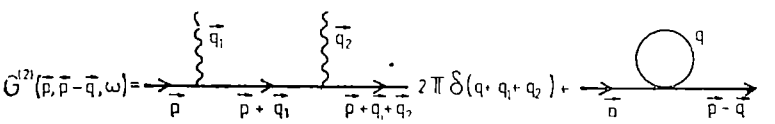

Fig 2

If we write now $\Delta_1(r)$ as

$$\Delta_1(r) = gT\pi \sum_n [\hat{G}(\vec{r}, \vec{r}, \omega) - \hat{G}_0(\vec{r}, \vec{r}, \omega)] \tag{14}$$

and consider the second order correction in A^2 to $\hat{G}$ we get for the Fourier transform

$$\left[g^{-1} - T\sum_n \int \frac{d^3\vec{p}}{(2\pi)^3} (G(\vec{p}, \omega) G^0(\vec{p}, \omega) - F^0(\vec{p}, \omega) F^0(\vec{p} + \vec{q}, \omega))\right] \Delta_1(r)$$

$$= \left(\frac{e}{m}\right)^2 T \sum_n \int \frac{d^3\vec{p}}{(2\pi)^3} \int \frac{dq_1\, dq_2}{2\pi} (\vec{p}\vec{A}(\vec{q})) (\vec{p}\vec{A}(\vec{q}_1)) [FFF +$$

$$+ GGG - GFG^+] \delta(q + q_1 + q_2) \tag{15}$$

The integral over $d^3\vec{p} = mp_c ded(\cos\theta) d\varphi$ can be performed and using relation

$$g^{-1} = \frac{mp_0}{2\pi^2} \ln \frac{2\omega_D}{\Delta(0)}$$

we get for (15)

$$L(q)\Delta_1(q) = \iint \frac{dq_1\, dq_2}{2\pi} L_2(q, q_1, q_2) A(\vec{q}_2) \delta(\vec{q} + q_1 + q_2) \tag{16}$$

where

$$L(q) = \sum_n \frac{1}{E} \left[1 - 2\frac{\omega^2}{qvE} \operatorname{arctang} \frac{vq}{2E}\right] \tag{17}$$

with $E^2 = \omega^2 + \Delta^2$.

For $q + q_1 + q_2 = 0$, L_2 has been calculated as

$$L_2(q) = \frac{\Delta}{2} (ev)^2 T \sum_n \frac{1}{E} \int d\mu (1 - \mu^2) \left\{\left[\frac{1}{(2\imath E - vq\mu)(2\imath E + vq_2\mu)} + \right.\right.$$

$$\left.\left. + \frac{1}{(2\imath E - vg\mu)(2\imath E + vq_2\mu)}\right]\left(1 - \frac{\Delta^2}{E^2}\right) - \frac{\Delta^2}{E^3} \frac{1}{(2\imath E + v\mu q_1)(\imath E - v\mu q_2)}\right\} \tag{18}$$

In the following we will consider penetration depth λ_L as being higher than coherence lenght ξ_0 (London superconductors) and we will approximate $L_2(q, q_1, q_2) \simeq L_2(q)$ Equation (17) becomes

$$\underset{q\to 0}{L(q)} = T \sum_n \frac{\Delta^2}{E^3} \tag{19}$$

and (18) will be

$$\underset{q\to 0}{L_2(q)} = -\frac{\Delta}{3} (ev)^2 T \sum_n \frac{1}{E^3} \tag{20}$$

Using these approximations Equation (16) will be written as

$$L(0)\Delta_1(\vec{r}) = -L_2(0)A^2(r) \tag{21}$$

which gives

$$\Delta_1(r) = -\frac{(evA(r)^2}{3\Delta}\left[\sum_n \frac{1}{\eta E^3}\right]\left[\sum_n \frac{1}{E^3}\right]^{-1} \tag{22}$$

and

$$\Delta_1(r)A(\Delta) = \frac{mp_0}{2\pi}\,\Delta\,\frac{(evA(r)^2}{3}\sum_n \frac{1}{\eta E^3} \tag{23}$$

where

$$\eta = 1 + \frac{1}{\tau\sqrt{\omega^2+\Delta^2}}\,\frac{1}{\tau} \cong \frac{1}{\tau_{tr}} = \int \mathrm{d}\Omega\,|V(\theta)|^2(1-\cos\theta)$$

Equation (23) has been obtained using transform $\Delta \to \eta\Delta$ $\omega \to \eta\Delta$ and taking $\tau^{-1} \ll \tau_{tr}^{-1}$.

With these approximations (23) becomes

$$\Delta_1(r)A(\Delta) = \frac{\pi\sigma}{32e^2r^2}\,\frac{d}{d\Delta(T)}\,\Delta(T)\tanh\left(\frac{\Delta(T)}{2T}\right)$$

where $\sigma = ne^2\tau_{tr}/m$ is the conductivity and $A(r)$ has been approximated as

$$A(r) = \frac{1}{2e\lambda_L}\,K_1(r/\lambda_L)$$

Energy E_v given by (8) will be

$$E_v = \frac{\pi^2\sigma}{4e^2}\left(\Delta(T)\tanh\frac{\Delta(T)}{2T}\right)\ln k(T) \tag{24}$$

and

$$E_1 = \frac{\pi^2\sigma}{4e^2}\left(\Delta(T)\tanh\frac{\Delta(T)}{2T}\right)\ln k(T) + \frac{\Phi_2^0}{32\pi^2\lambda_L^2(T)} \tag{25}$$

The lower critical field H_{c1} can be calculated from (1) as

$$H_{c1}(T) = \frac{4\pi}{\Phi_0}\left[\frac{\pi^2\sigma}{4e^2}\left(\Delta(T)\tanh\frac{\Delta(T)}{2T}\right)\ln k(T) + \frac{\Phi_0^2}{32\pi^2\lambda_L^2}\right] \tag{26}$$

which is the general equation for type—II superconductors.

Lower Critical Field for an Antiferromagnetic Superconductor. In order to apply these results to a antiferromagnetic superconductor we will write Equation (23) as

$$\Delta_1(r)A(\Delta) = \frac{mp_0}{2\pi}\,\Delta\tau_{tr}\,\frac{(evA(\vec{r}))^2}{3}\sum_n \frac{E^2}{E^4} \tag{27}$$

and $E^2 = \omega^2 + \Delta^2(r) + M^2(T)$ where $M(T)$ is the sublattice magnetization [6].

Equation (27) becomes

$$\Delta_1(r)A(\Delta) \sim (N_1(r)A(\Delta)) + \frac{mP_0}{6\pi}\Delta\tau_{tr}M^2(T)H\sum_n \frac{1}{E^4} \tag{28}$$

where we denoted $\tilde{\Delta}^2 = \Delta^2 + M^2$

A last summation can be performed and we get

$$\Delta_1(r)A(\tilde{\Delta}) = \Delta_1(r)A(\tilde{\Delta}) - \frac{mp_0}{6\pi}\Delta\tau_{tr}(evA(r))^2M^2(T) +$$

$$+ \frac{\Delta(0)}{\Delta(T)}\frac{d}{d\Delta(T)}\left(\frac{\Delta(0)}{\Delta(T)}\tanh\frac{\Delta(T)}{2T}\right)$$

and the lower critical field $H_{c1}^a(T)$ becomes

$$H_{c1}^a = H_{c1} + \left[\frac{\pi^3\sigma}{e^2\Phi_0}\left(\frac{\Delta(0)}{\Delta(T)}M(T)\right)^2\tanh\frac{\Delta(T)}{2T}\right] \tag{29}$$

where H_{c1} is given by (26)

The generalization for the spin-glass superconductor can be performed, if τ_{tr} is considered for a random spin distribution in a superconductor and τ_{tr}^{-1} will be averaged using the method given by Crişan *et al* [7]

REFERENCES

1 A A Abrikosov, *JETF* **32,** 1442 (1957)

2 C Caroli, P G de Gennes and P. Matricon, *Phys Lett*, **9,** 307 (1964)

3 M Tachiki, H Matsumoto and H Umezwa a, *Phys Rev*, **B 20,** 1915 (1979), S Maekawa, M Tachiki and S Takahashi, J *Magnetidsm Mag Materials*, **13,** (1979)

4. H Matsumoto, R Teshima, H Umezawa and M Tachiki, *Phys Rev*, **B 27,** 158 (1983); H Matsumoto, H Umezawa and J. P. Whitheded, *Phys Rev*, **B 30,** 1294 (1983), *J. P Whithehead*, H. Matsumoto, R. Teshima and Umezawa, *Phys Rev*, **30,** 1314 (1984)

5 A. E. Jacobs, *JLTP*, **10,** 137 (1973)

6 M Crişan, Zs Gulacsi and Al Anghel, „Proc 16-th, Int Conf. on Low Temp II", *Physica*, **B + C 107,**, 1049 (1981)

7 M Crişan, M Gulacsiand Zs Gulacsi, „Proc 17-th Int Conf on Low Temp II", 1984, Karlsruhe, p 1865

STUDIA UNIV BABEŞ—BOLYAI, PHYSICA, XXXI, 2, 1986

DIMENSIONS OF THE GENERALIZED BAKER'S TRANSFORMATION

STELIANA CODREANU* and CONSTANTIN CODREANU**

Received February 12, 1986

ABSTRACT. — An efficient method for computing the dimensions of the attractor associated with Baker's transformation is presented.

In this paper we report a rapid method for computing capacity dimension d_c, and information dimension d_i [1] of the attractor associated with generalized Baker's transformation

The generalized Baker's transformation is defined by the map

$$x_{n+1} = \begin{cases} a x_n & \text{if } y_n < c \\ \frac{1}{2} + b x_n & \text{if } y_n > c \,, \end{cases}$$

$$y_{n+1} = \begin{cases} \frac{1}{C}\, y_n & \text{if } y_n < c \\ \frac{1}{1-C}\,(y_n - c) & \text{if } y_n > c \,, \end{cases} \tag{1}$$

where $0 \leqslant x_n \leqslant 1$ and $0 \leqslant y_n \leqslant 1$

Figures 1 (a) and (b) illustrate the action of this map on the unit square, with $a,\ b,\ c \leqslant \frac{1}{2}$ and $b \geqslant c$ Figure 1 (c) shows the result of applying the map two times to the unit square We can see from Figure 1(c) that if the x — interval $[0,\ a]$ is magnified by a factor $1/a$, or if the x — interval $[1/2,\ 1/2,\ +b]$ is magnified by $1/b$, one onbtains a replica of Fig 1(b) Each part of the obtained map is equivalent to the original map This self similarity property of the map may be used to obtain d_c and d_i

By examining the construction of Figure 1(b) and (c), one observes that we are in the process of constructing a Cantor set along x Hence the attractor is a product of a Cantor set along x and the interval $[0,\ 1]$ along y Thus the capacity dimension and the information dimension are in the form

$$d_c = 1 + \bar{d}_c\,, \qquad d_i = 1 + \bar{d}_i \tag{2}$$

where $\bar{d}_c$ and $\bar{d}_i$ are the dimensions of the attractor in the x — direction.

* *University of Cluj-Napoca, Department of Physics, 3400 Cluj-Napoca, Romania*
** *Polyt Inst of Cluj-Napoca, 3400 Cluj-Napoca, Romania*

To obtain $\bar{d}_c$ and $\bar{d}_i$ for this Cantor set one uses the relations indicated by Shau—Jin Chang and J Mc Cown [2], for Feigenbaum attractors

$$\sum_{i=1}^{n} q_i^{\bar{d}_c} = 1 \tag{3}$$

and

$$\bar{d}_i = \frac{\sum_{i=1}^{n} p_i ln \frac{1}{p_i}}{\sum_{i=1}^{n} p_i ln \frac{1}{q_i}} \tag{4}$$

where $q_i (i = 1, \quad , n)$ are the lengths of subintervals of the x — interval [0, 1] on Figure 1(b), and and p_i is the probability of the attractor to be in the subinterval q_i

Thus from (3) one finds

$$a^{\bar{d}_c} + b^{\bar{d}_c} = 1$$

which is the equation for $\bar{d}_c$, and from (4) one finds

$$d_i = \frac{c ln \frac{1}{c} + (1 - c) ln \frac{1}{1 - c}}{c ln \frac{1}{a} + (1 - c) ln \frac{1}{b}} = \frac{H(c)}{c ln \frac{1}{a} + (1 - c) ln \frac{1}{b}}$$

where H(c) is the binary entropy function

These results coincide with those obtained by J D Farmer *et al* [1] by the box counting method

It is interesting to remark that relations (3) end (4) can be used to calculated the capacity and the information dimension of an asymmetric Cantor set [3] Let the Cantor set be made by deleting the third fourth of the interval [0, 1], then deleting the third fourth of each remaining piece, and so on (see Fig 2)

This Cantor set is self-similar, i e each of its subintervals is identical to its original interval up to a scaling

By using (3), the capacity is found from equation

$$\left(\frac{1}{2}\right)^{d_c} + \left(\frac{1}{4}\right)^{d_c} = 1$$

This gives

$$d_c = \frac{ln\ 1\,618}{ln\ 2} = 0{,}694$$

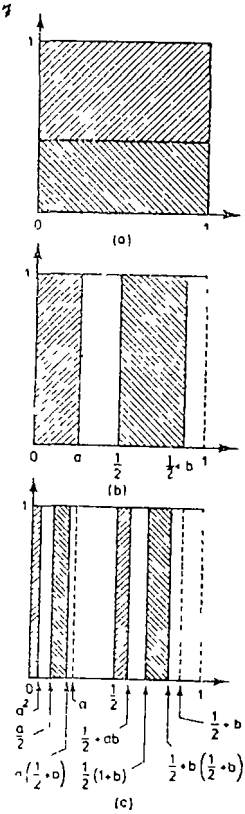

Fig. 1 The generalized Baker's transformation The action of the map on unit square (one iteration) is shown from (a) to (b) The result of applying the map two times to the unit square (second iteration) is shown in (c)

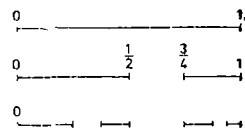

Fig 2 The geometrical construction of an asymetric Cantor set.

To calculate d_c by the box counting method if one uses the considerations made by J.D. Farmer *et al.* [1], one finds the same result and not log 3/log 4 = = 0,792 as is indicated in the paper [4]

For d_t, by using (4), one obtains

$$d_t = \frac{\frac{2}{3} ln \frac{3}{2} + \frac{1}{3} ln 3}{\frac{2}{3} ln 2 + \frac{1}{3} ln 4} = \frac{3}{4} \frac{H\left(\frac{1}{3}\right)}{ln 2} = 0{,}688$$

which coincides with J.D. Farmer's result [4].

REFERENCES

1. Farmer J D, Ott E, and Yorke J A „The dimensions of chaotic attractors", *Physica D*, vol **7**, 153, (1983)
2. Shau-Jin Chang and John Mc Cown „Universal exponents and fractal dimensions of Feigenbaum attractors", *Physical Review A*, vol 30, **2**, 1149, (1984)
3. Codreanu S „Dimensiunile unui set Cantor asimetric", *Progrese în fizica*", **292**, (1985)
4. Farmer J D. „Information Dimension and the Probabilistic Structure of Chaos", *Z. Naturforsch*, **37**a, 1304, (1982)

STUDIA UNIV BABEŞ—BOLYAI, PHYSICA, XXXI, 2, 1986

ELECTRONIC SEMICONDUCTOR REZISTANCE MEASURER BASED ON IMPULSE EXCITATION

F. PUSKAS*, S. SELINGER** and F. F. PUSKAS***

Reeceived October 13, 1986

ABSTRACT. — An electronic instrument is presented, that uses impuls excitation for semiconductor rezistance measuring The method eliminates the errors caused by thermo-, photo-electrical, contact and polarization phenomena, which sometimes may occur between electrodes and semiconductor sample.

The instrument presented below, using double polar impulses, avoids rezistance measureing error possibilities due to thermo-, photo-electrical, contact and polarization phenomena.

It is a perfected model of the electro-mechanical appliance described in [1—4], by using solid state devices instead of electro-mechanical components.

Operating principle. To the measuring circuit (Fig. 1) we apply the impulses given by a square-wave oscillator. It's waveform is shown in (Fig. 2). The R standard adjustable rezistance is crossed by the same current as the P semiconductor sample. The C_1 and C_2 capacitors are alternatively charged through K_1 and K_2 electronic switches to U_R and U_P charging voltages.

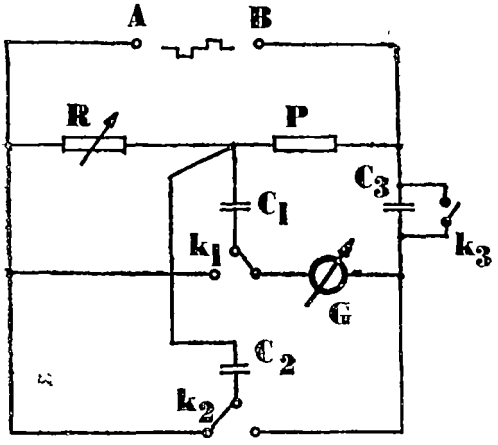

Fig 1 Measuring circuit.

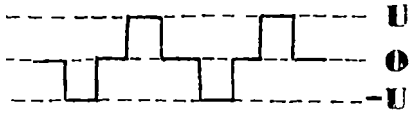

Fig. 2 Waveform given by the impulse generator

The polarity of U_R and U_P is not changing, because while the K_1 and K_2 switches are swiching in and off the polarity of the alternating current mains is changing simultaneously. It's easy to understand that if C_3 is short-circuited and $U_R = U_P$ then the G galvanometer is crossed by a current.

* *University of Cluj-Napoca, 3400 Cluj-Napoca, Romania*
** *ITC—Cluj-Napoca, 3400 Cluj-Napoca, Romania*
*** *IAUC — Cluj-Napoca, 3400 Cluj-Napoca, Romania*

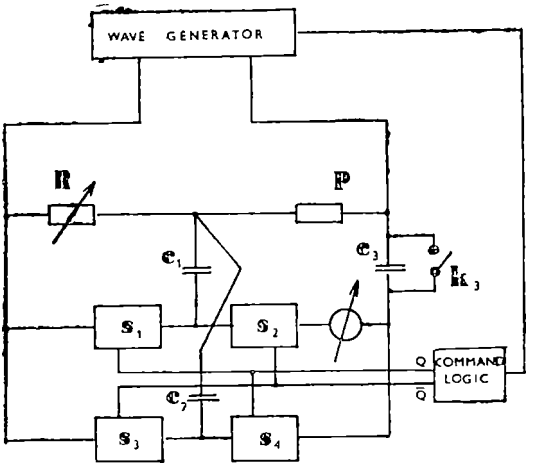

Fig 3 The block diagram of the electronic circuit

The $U_R = U_P$ condition can be reached by modifying R, in this case the G galvanometer will indicate no current, because the C_1 and C_2 capacitors are connected to the same voltage, thereby the galvanometer will indicate no charging or discharging current Naturally, the condition of this state of balance equilibrium is $R = P$. It is proved [4] that this condition is unchanged even if C_3 is not short-circuited and the probe head introduces contact electricity.

The block diagram of the electronic instrument is shown in (Fig 3)

The rectangular impulses were generated by the help of an integrated oscillator 555NE, combined with a schematic of transistors, and an IC—CD4016 was used as switch.

The sensibility of the bridge grew by increasing the frequency of the rectangular impulses By changing the frequency from 1 kHz to 10 kHz it was found out a certain increase of the measuring field from 100 kΩ to $M\Omega$.

REFERENCES

1. T. M Dauphinee, Can J. Phys, **31**, 577 (1953)
2. T. M. Dauphinee, S B. Woods, Rev Sci Instr, **26**, 660 (1955)
3. T M. Dauphinee, S. B Woods, Rev Sci Instr, **26**, 693 (1955)
4 F Puskas, Gh Ilonca, Studii şi Cerc de Fizică, **19**, 165 (1967)

STUDIA UNIV BABEŞ—BOLYAI, PHYSICA, XXXI, 2, 1986

STATISTICAL EQUILIBRIUM OF METASTABLE STATES

M. CRIŞAN*

Received October 20, 1986

ABSTRACT — A procedure is outlined for the general condition of the statistical equilibrium of the systems described by the Fokker-Plank equation The method provides a definite prescription for the study of the equilibrium for the metastable states near the saddle point

1 **Introduction.** The classical theory for a metastable state has been given in 1935 by Becker and Doring [1] for the system consisting fo supersaturated vapor This theory has been generalized by Landauer and Swanson [2] and generalized for superfluidity by Langer and Fisher [3] and superconductivity by Langer and Ambegaokar [4] In the last two quantum phenomena the states of nonzero superflow are metastable and, as the supersaturated vapor, may undergo spontaneous transitions to states of lower current and greater stability

The statistical theory of metastable states has been generalized by Langer [5] for the systems which have and own dynamics described by

$$\frac{dx_i(t)}{dt} = \sum_j A_{ij} \frac{\partial E}{\partial x_i} \tag{1}$$

where $x_i(t)$ are the relevant variables (average magnetization the superconducting order parameter, density) and A_{ij} is an antisymmetric matrix.
The distribution function $P(x, t)$, where $x = (x_1(t) \ \ldots \ x_n(t))$ can be obtained from the Fokker—Planck equation

$$\frac{\partial P(x, t)}{\partial t} = -\sum_i \frac{\partial J_i}{\partial x_i} \tag{2}$$

where J_i is the i'th component of the probability-current density and is expressed as

$$J_i = -\sum_j M_j \left(\frac{\partial E}{\partial x_i} P + kT \frac{\partial P}{\partial x_i} \right) \tag{3}$$

where

$$M_{ij} = \frac{\Gamma_i}{KT} \delta_{ij} - A_{ij} \tag{4}$$

The equilibrium solution of (2) having the from

$$P_0(x) \sim \exp\left[-E(x)/kT\right] \tag{5}$$

* *University of Cluj-Napoca, Department of Physics, 3400 Cluj-Napoca, Romania*

(corresponding to $J_i = 0$ for all i) describes the stable states. The stable and metastable states occur near the position of the local minima of $E(x)$ and the important tranzition is between such two minima. This transition between two minima is most likely to pass across the lowest saddle point of the function $E(x)$. Generally this saddle point, denoted by $\tilde{x}$ will describe a configuration which is identical with every state where the initial metastable state except for the presence of a single localized fluctuation In the case of the supersaturated vapor this is a droplet or a vortex ring for a superfluid. Once x reaches $\tilde{x}$ a greater stability has been attended and x describes the fluctuations which nucleates the phase transition.

The problem which appears now is to demonstrate the existence of another solution for (2) which is different from (5) and describes the finite probability current flowing across the saddle point $\tilde{x}$.

2. **Necessary condition — the equilibrium.** We will look for a condition of the statistical equilibrium in the imediate neighbourhood of the sadle point x. Langer [5] pointed out that a Fokker—Planck equation near the saddle point can be obtained if we perform the transform

$$y_n = \sum_i D_{ni}(x_i - \bar{x}_i) \tag{6}$$

where D is an ortogonal transform which has been chosen so that near $x = 0$ the energy $E(x)$ can be expended as

$$E(x) = \bar{E} + \frac{1}{2}\sum_{n=1}^{2N} \lambda_n x_n^2 \tag{7}$$

where $E = \bar{E}(\bar{x})$ and λ_n are eigenvalues of the matrix $\partial^2 E/\partial x_i \partial x_j$ evaluated at $\bar{x}$. These eigenvalues are sensitive to the symmetry of the system but near the saddle point x these is always a nonzero eigenvalue which is negative. In fact the saddle point is a bounded, finite-dimensional subspace of x-space. In the new coordinate system the current (3) becomes

$$\tilde{J}_n = \sum_n D_{ni} J_i = -\sum_{n'} \tilde{M}_{nn'} \left(\frac{\partial E}{\partial y_{n'}} + kT \frac{\partial P}{\partial y_{n'}} \right) \tag{8}$$

where

$$M_{nn'} = \sum_{ij} D_{ni} M_{ij} D_{n'j} \equiv \frac{1}{kT} \tilde{\Gamma}_{nn'} - \tilde{A}_{nn'} \tag{9}$$

The steady-state solutions of (2) can be obtained from the equation

$$\sum_{n=1}^{m} \frac{\partial \tilde{J}}{\partial y_n} = -\sum_{n',n=1}^{m} \frac{\partial}{\partial y_n} \left[\tilde{M}_{nn'} \left| \frac{\partial E}{\partial y_{n'}} P + kT \frac{\partial P}{\partial y_{n'}} \right) \right] \tag{10}$$

equation which will be written as

$$\sum_{=1}^{m} \frac{\partial}{\partial y_n} (K_n P) + \sum_{n,n'=1}^{m} \tilde{M}_{nn'} kT \frac{\partial P}{\partial y_n \partial y_{n'}} = 0 \tag{11}$$

where

$$K_n(y) = \sum_{n'=1}^{m} \tilde{M}_{n,n'} \frac{\partial E}{\partial y_{n'}} \tag{12}$$

A solution of the equation (2) satisfies

$$0 \leqslant P(y,\ t) < \infty \tag{13.a}$$

$$\int \mathrm{d}^m y P(y,\ t) = 1 \tag{13.b}$$

The last equation shows that $P(y,\ t)$ is normalizable in $\mathcal{R}_m$ i.e. P has to be a function in $L^1_+(\mathcal{R}_m)$ The equation (10) will be written as

$$-\sum_{n=1}^{m} \int \mathrm{d}^m y \frac{\partial}{\partial y_n} [K_n(y)P]P = \sum_{n',n=1}^{m} \tilde{M}_{n,n'} kT \int \mathrm{d}^m y P \frac{\partial^2 P}{\partial y_n \partial y_{n'}} \tag{14}$$

which can be transformed in

$$-\int \mathrm{d}^m y S P^2(y) = \sum_{n,'n}^{m} kT\tilde{M}_{n,n'} \int \mathrm{d}^m y \frac{\partial P}{\partial y_n} \frac{\partial P}{\partial y_{n'}} \tag{15}$$

where

$$S = S(y) = \sum_{n=1}^{m} \frac{\partial K_m(y)}{\partial y_n} \tag{16}$$

The left side of the equation (14) is bounded from above by applying the Holder inequality

$$-\int \mathrm{d}^m y S(y) P^2(y) \leqslant \int_{\Omega} \mathrm{d}^m y\, |S|P^2(y) \leqslant \left(\int_{\Omega} \mathrm{d}^m y\, |S|^{\frac{m}{2}}\right)^{\frac{2}{m}} \left(\int_{\Omega} \mathrm{d}y^m P(y)^{\frac{2m}{m-2}}\right)^{\frac{m-2}{m}} \tag{17}$$

where Ω is a subspace defined as: $\Omega \equiv \{y \subset \mathcal{R}_m\}$ such that $S < 0$. From (12) and (16) we see that this is an agreement with the existence of a subspace so that any eigenvalues λ_i are negative. The right side of the equation (14) is bounded from below by applying the Sobolev inequality

$$\sum_{i=1}^{m} \int \mathrm{d}^m z \left(\frac{\partial f}{\partial z_i}\right)^2 \geqslant c_m \left(\int \mathrm{d}^m z\, |f|^{\frac{2m}{m-2}}\right)^{\frac{m-2}{m}} \tag{18}$$

where

$$c_m = 2^{-2+\frac{2}{m}} \pi^{1+\frac{1}{m}} (m^2 - m) \left[\Gamma\left(\frac{m+1}{2}\right)\right]^{-\frac{2}{m}} \tag{19}$$

Taking $\mathrm{f} = P(y)$ and $x_n = \sum^{k} (M^{1/2})_{n,k} y_k$ one obtains

$$\sum_{n,n'=1}^{m} kT\tilde{M}_{n,n'} \int \mathrm{d}^m y \frac{\partial P}{\partial y_n} \frac{\partial P}{\partial y_{n'}} > c_n M \left(\int \mathrm{d}^m y P(y)^{2m/(m-2)}\right)^{(m-2)/m} \tag{20}$$

where $\mathrm{M} = (\det \mathrm{M}_{n,n'})^{1/m}$.

Strict inequality is indicated in (19) because P is defined as function in $L^1_+(\mathcal{R}_m)$. From (14), (17) and (19) we get the equilibrium condition as

$$\left(\int_{\Omega} d^m y \, |S|^{\frac{m}{2}}\right)^{\frac{2}{m}} > \frac{1}{kT} \, c_m M \tag{21}$$

From (19) we get

$$C_m > 4 \cdot 2699 \ (m-2) \text{ if } m \geqslant 3$$

and

$$\lim_{m\to\infty} \frac{C_m}{m} = 4 \cdot 2699$$

Discussions. The condition (21) assures the existence of the solution for the Fokker—Planck equation near the saddle-point associated with a metastable state. This inequality is satisfied if $S < 0$ and sufficiently large in absolute magnitude for $\Omega \subset \mathcal{R}_m$ On the other hand in the expansion (7) we need a negative eigenvalue to be sure that $S < 0$, and we have a solution if (2) is in the immediate neighbourhood of the saddle-point $\bar{x}$

REFERENCES

1. R. Becker and W. Döring, Ann Physik, **24**, 719 (1935)
2. R. Landauer and J. A Swanson, Phys Rev, **121**, 1668 (1961)
3. J. S. Langer and M. E Fisher, Phys Rev Letters, **19**, 560 (1967)
4. J. S. Langer and V. Ambegaokar, Phys Rev, **164**, 498 (1967)
5. J. S Langer, Ann Phys (N.Y) **54**, 258 (1969)

STUDIA UNIV BABEŞ—BOLYAI, PHYSICA, XXXI, 2, 1986

EFFECT OF CONCENTRATION FLUCTUATIONS ON THE CRITICAL TEMPERATURE OF SUPERCONDUCTING PAIRING IN BINARY ALLOYS

I. GROSU* and M. CRIŞAN*

Received October 21, 1986

ABSTRACT. — The influence of the phonons and electron-hole excitation has been studied in the superconductivity given by a nonphononic interaction Particulary, this mechanism is given by the concentration waves which may appear in the binary ordered alloys

Introduction. We consider a periodical-spatially ordered alloys A_xB_{1-x} where the concentration of the atoms A is $c(\vec{r})$ and of the atom B is $1 - c(\vec{r})$ This system can be described by fermionic operators $\alpha_i^+(\vec{r})$ and $\alpha_i(\vec{r})$ which describes the creation and destruction of an atom of kind A in the point r in the sublattice „i". The Hamiltonian which describes the concentration fluctuation has the form

$$H = \frac{1}{2}\sum_{\vec{r},\vec{r}'} W(\vec{r} - \vec{r}')\delta\hat{c}(\vec{r})\delta\hat{c}(\vec{r}) \tag{1}$$

where

$$\delta\hat{c}(\vec{r}) = \frac{1}{2}\sqrt{c(1-c)}(\hat{\varphi}^+(\vec{r}) + \hat{\varphi}(\vec{r})) \tag{2}$$

and

$$\hat{\varphi}(\vec{r}) = \sum_{\vec{k}} \varphi_{\vec{k}}(\vec{r})\hat{\alpha}_k$$

If we introduce now the operators

$$b(\vec{r}) = \alpha_1^+(\vec{r})\alpha_2(\vec{r}) \quad b^+(\vec{r}) = \alpha_2^+(\vec{r})\alpha_1(\vec{r}) \tag{3}$$

the Hamiltonian (1) can be transformed as

$$H_c = \sum_{\vec{k}} \frac{1}{8} c(1-c)W(\vec{k})\,[2b_{\vec{k}}^+ b_{\vec{k}} + b_{-\vec{k}}^+ b_{\vec{k}} + b_{-\vec{k}}^+ b_{\vec{k}} - \mu b_k^+ b_k] \tag{4}$$

where $W(\vec{k})$ is the Fourier transform of $W(\vec{r} - \vec{r}')$, c is the concentration of the atoms in the sublattice A and μ is the chemical potential This hamiltonian has been diagonalized [4] using a unitar transform and

$$H_c = \sum_{\vec{k}} \omega_c(\vec{k})\, c_{\vec{k}}^+ c_{\vec{k}} \tag{5}$$

* *University of Cluj-Napoca, Department of Physics, 3400 Cluj-Napoca, Romania*

where the operators $c_{\vec{k}}^{\pm}$ and $c_{\vec{k}}$ describes the bozonic excitations due to concentration fluctuations and $\omega_c(\vec{k})$ is the energy of these excitations given as

$$\omega_c(\vec{k}) = \left[\mu^2 - \mu c(1-c)W(k)\,\frac{1}{2}\right]^{1/2} \tag{6}$$

If one defines the number of "bosons" due to the fluctuations $N_s = b_{ks}^{+} b_{\vec{ks}}$ the energy (6) has been expanded as

$$\omega_c(\vec{k}) \cong \frac{1}{4}\, c(1-c)W(\vec{k}) - \mu$$

or if we introduce

$$\vec{q} = \vec{k} - \vec{k}_s,\ W(\vec{q}) \cong W(k_s) + \gamma q^2$$

the equation (6) becomes

$$\omega_c(q) = \Delta + \frac{1}{4}\, c(1-c)\gamma q^2 \tag{7}$$

where

$$\gamma \cong \gamma_0 |W(k_s)|,\ \Delta \cong \frac{1}{4}\, c(1-c)W(k_s) - \mu$$

The interaction between this excitations and electrons can be described by the Hamiltonian

$$H_{e-c} = \int d\vec{r} \sum_{k} [V_A(\vec{r} - R) - V_B(\vec{r} - \vec{R})]\, \varphi^{+}(\vec{r})\, \varphi(\vec{r})\, \delta\hat{c}(\vec{r}) \tag{8}$$

which becomes

$$H_{e-c} = \int d\vec{r} \sum_{\vec{k},\vec{q}} g(\vec{q})\, [a_{k+q}^{+} a_k b_q + a_k^{+} a_{k+q} b_q^{+}] \tag{9}$$

where

$$g(\vec{q}) = \frac{1}{2N}\sqrt{c(1-c)}\,(V_A(\vec{q}) - V_B(\vec{q}))$$

The Hamiltonian (9) contains terms with $\vec{q} = \vec{k}_s$ which will give a state similar with "superfluidity" and terms with $\vec{q} \neq \vec{k}_s$ which may give rise to an effective interaction

$$H_{eff} = \sum_{\vec{k},\vec{k}',\vec{q}=\vec{k}_0} \frac{|\mu|}{(\varepsilon(k+q) - \varepsilon(k))^2 - \omega_c^2(q)}\, a_{\vec{k}+\vec{q}}^{+} a_{\vec{k}'-\vec{q}}^{+} a_{\vec{k}} a_{\vec{k}'} \tag{10}$$

which becomes attractive if $\varepsilon(\vec{k} + \vec{q}) - \varepsilon(\vec{k}) < -\omega_c(\vec{q})$.

In order to describe the superconducting state we have to define the Green function for the quasiparticles associated with the concentration fluctuations. If we define the operator

$$\hat{\Phi}(\vec{r},\ t) = \sum_{\vec{R}} g(\vec{r} - \vec{R}) \sqrt{\frac{c(1-c)}{4}}\ (\hat{\varphi}^{+}(\vec{R},\ t) + \hat{\varphi}(\vec{R},\ t)) \tag{11}$$

the Green function

$$D(\vec{r}t\,;\ \vec{r}'t') = \langle T\Phi(\vec{r},\ t)\Phi(\vec{r}'t')\rangle$$

with the Fourier transform

$$D(\vec{q},\ \omega_n) = \frac{c(1-c)}{2\rho}\ \frac{g^2(q)}{(i\omega_n)^2 - \omega_c^2(q)} \tag{12}$$

will describe the free quasiparticle associated with the concentration variation.

Eliashberg Equation. We consider the electron-phonon, the Coulombian interaction and the interaction between electrons and quasiparticles associated with the concentration variation. Following the standard procedure [2] we get

$$Z(\omega)\Delta(\omega) = \int_{-\infty}^{\infty} dz' [K_{ph}(z',\ \omega) + K_c(z',\ \omega) - K_m(z',\ \omega)]\ \mathrm{Re}\left\{\frac{\Delta(z')\ \mathrm{sign}\ z'}{\sqrt{z'^2 - \Delta^2(z')}}\right\} \tag{13}$$

$$[1 - Z(\omega)]\Delta(\omega) = -\int_{-\infty}^{\infty} dz' [K_{ph}(z',\ \omega) + K_c(z',\ \omega) - K_m(z',\ \omega)]\ Re\left\{\frac{\Delta(z')\ \mathrm{sign}\ z'}{\sqrt{z'^2\Delta^2(z')}}\right\} \tag{14}$$

where the general form of the kernel $K\ (z,\ \omega)$ is

$$K_i(z',\ \omega) = \int_0^{\infty} dz\alpha_i^2(z)F_i^2(z)\ \frac{1}{2}\left[\frac{\tanh\frac{z'}{2T} - \mathrm{cotgh}\frac{z}{2T}}{\omega + z - z' + i\delta} - \frac{\tanh\frac{z'}{2T} + \mathrm{cotgh}\frac{z}{2T}}{\omega - z + z' + i\delta}\right] \tag{15}$$

where "i" denotes the phononic contribution, the contribution of the concentration and the contribution of the magnetic fluctuations studied by Berk and Schrieffer [3].

In order to calculate the critical temperature we consider the weak — coupling limit and (15) can be approximated as

$$K_i(z',\ 0) = 2\int_0^{\infty} dz\ \frac{\alpha_i^2(z)F_i(z)}{2}\ \frac{1}{2}\tanh\frac{z'}{2T} = \frac{\lambda_i}{2}\tanh\frac{z'}{2T} \tag{16}$$

The parameters λ_{ph}, λ_m have been given for conventional theory of the strong-coupling superconductors and

$$\lambda_c = 2f(c)\int_0^{z} dz\frac{\alpha_c^2(z)\,F(z)}{2} \tag{17}$$

where

$$\alpha_c^2(z)F(z) = \int_{S_F} \frac{d^2\vec{p}}{v_p} \int_{S_{F'}} \frac{d^2\vec{p}'}{v_p} f(c)\,|g_c(\vec{p},\ \vec{p}')\,|^2\delta(z - \omega_c(q)) \left(\int_{S_F} \frac{d^2\vec{p}}{v_{\vec{p}}}\right)^{-1} \tag{18}$$

$$f(c) = \frac{c(1-c)}{2\rho}$$

The equations (13—14) have been solved in the weak coupling approximation using the ansatz

$$\Delta(\omega) = \begin{cases} \Delta_{ph} & |\omega| < \omega_D \\ \Delta_c & |\omega| < \omega_0 \\ \Delta_v & \omega_0 < |\omega| < \omega_w \end{cases} \tag{19}$$

and the critical temperature becomes

$$T_c = 1.134 \exp\left[-\frac{1}{\lambda_{ph} + \lambda_c - \lambda_m}\right] \tag{20}$$

The parameter λ_m has been calculated a $T = 0$ in the t-matrix [3] approximation as

$$\lambda_m = aU_cN(0)ln\frac{1}{1 - U_cN(0)} \tag{21}$$

where $a = 2$ if $U_cN(0) \cong 1$ and $a = 1$ if $U_cN(0) \ll 1$.
These results are similar with the recent results obtained in [4] but for $\lambda_c = 0$ and $\lambda_m = \mu_c^*$.

The effect of the concentration fluctuations on the critical temperature. The equations (13—14) will be written on the imaginary-frequency axis and (13—14) becomes

$$\Phi(i\omega_n) = \pi T_c \sum_{m=0}^{\infty} \frac{\Delta(i\omega_m)}{\omega_m} [\lambda_v\theta(\omega_c - \omega_m) + \lambda_{n-m} + \lambda_{n+m+1}] \tag{22}$$

$$Z(i\omega_n) = 1 + \frac{\pi T_c}{\omega}\left[\lambda_0 + 2\sum_{m=1}^{\infty} \lambda_m\right] \tag{23}$$

where

$$\lambda_u = \frac{\lambda_m}{2} = K_m(0,\ 0) \tag{24}$$

$$\lambda_i = \lambda_{ph} + \lambda_c \qquad i = \in [m,\ \infty)$$

and we introduced $\Delta(i\omega_n) = \Phi(i\omega)/Z(i\omega_n)$ where λ_n is expressed by

$$\lambda_i(m) = 2\int_0^{\infty} \frac{d\Omega\ \alpha_{ph}^2(\Omega)F_{pg}(\Omega)}{\Omega^2 + (2\pi m T_c)^2} + 2f(c)\int_0^{\infty} \frac{d\Omega\alpha_c^2\,(\Omega)F_c(\Omega)}{\Omega^2 + (2\pi m T_c)^2} \tag{25}$$

If we consider the phonons and concentration contributions having the same order of magnitude and introduce the parameter

$$x = \frac{2}{(2\pi T_c)^2}\int_0^\infty d\Omega\alpha^2(\Omega)F(\Omega) \tag{26}$$

this is a small parameter for $2\pi T_c \gg \Omega$.
The solution of (22—23) becomes

$$\Delta(i\omega_n) = \sum_{m=0}^{\infty}\frac{\Delta(i\omega n)}{2m+1}\left[\lambda_u\theta(\omega_c - \omega_m) + x(f(c)+1)s_{n,m}\right] \tag{27}$$

where

$$s_{n,m} = \frac{1-\delta_{n,m}}{(n-m)^2} + \frac{1}{(n+m+1)^2} - 2\delta_{n,m}\sum_{m'=1}^{\infty}\frac{1}{n'^2} \tag{28}$$

and let us consider

$$\Delta(i\omega_n) = \Delta(i\omega_c)(1+\delta_n), \quad |\delta_n| \ll 1 \tag{29}$$

The critical temperature will be calculate taking $\delta_n \cong \delta_0$ and we get after some algebra

$$\frac{T_c}{T_{c0}} = \exp\left[\frac{4\,057x(f(c)+1)}{1-1\,545x(f(c)+1)}\right] \tag{30}$$

where T_c^0 is the critical temperature defined by

$$1 = \lambda_u(\omega_c)\sum_{m=0}^{m_c^0}\frac{1}{m+\frac{1}{2}}$$

and we used

$$\sum_{m=0}^{m_c}\frac{1}{m+\frac{1}{2}} - \sum_{m=0}^{m_c^0}\frac{1}{m+\frac{1}{2}} \cong ln\frac{T_c^0}{T_c}$$

The temperature T_c^0 can be considered as the critical temperature of a superconducting state mediated by the dinamycal spin-fluctuations and the equation (30) shows the influence of the concentration fluctuations on the critical temperature T_c for an ordered alloy A_xB_{1-x}.

Conclusions. We showed that in the model for the superconducting pairing in a crystalline ordered alloy A_xB_{1-x} the concentration fluctuations can give rise to a decreasing of the critical temperature. The effect is similar with

the thermal phonons. We neglected the influence of these fluctuations on the pseudopotential μ_c^* because in this model a separat analysis for this problem is necessary, but we considered the electron-hole scattering which may be important in this alloys

REFERENCES

1. A. I. Olemskoi, FMM. **51,** 917 (1981)
2. S V. Vonsovskii, Yu A Izumov and E. Z Kurmaev „Superconductivity of Tranzition Metals" Springer-Verlag, Berlin, Heidelberg 1982 pag 44
3 N F. Berk and J. R. Schrieffer, Phys Rev Lett **17,** 1171 (1966)
4. V E. Egorushkin and A. I Murzaschev, FTT. **12,** 3526 (1985)

STUDIA UNIV BABEŞ—BOLYAI, PHYSICA, XXXI, 2, 1986

MAGNETIC BEHAVIOUR OF V-Fe SOLID SOLUTIONS

LILIANA POP*, TEOFIL CHEREBEŢIU* and IULIU POP*

Received October 31, 1986

ABSTRACT. — The V—Fe solid solutions in α and σ-phases were investigated from a magnetic point of view between 100 — 1300 K For the samples containing 91, 88 and 79 at % V the magnetic susceptibility is temperature independent, i e this samples are Pauli paramagnets For the other samples containing 72, 68, 55 and 46 at %, V, the temperature dependence of the reciprocal magnetic susceptibility is not linear and obey the Néel law for the paramagnetic susceptibility of the ferrimagnetic ordered materials The effectiv magnetic moment determined per iron and vanadium atoms are in good agreement whith the values obtained in pure iron and for V^{+2} ion, at low temperature, the last sample exhibits the mixed valence characteristic, perhaps

Introduction. The V-Fe system of alloys has a continuous α solid solubility, excepting the central σ phase below 1200°C, and the iron narrow γ phase region [1, 2] According to phase diagram [1], σ phase is includid between 38 at. %⁻V and 58 at. % V. At the equiatomic concentration a FV intermetallic compound is formed. The σ solid solutions are ordered with FV intermetallic compound crystalline structure.

From a magnetic point of view, the iron rich solid solutions are ferromagnetics, and concentration dependence of the Curie temperature is reported on both phase diagrams [1, 2] but on the phase diagram [2] the concentration dependence is extended over the σ — phase until T = 0°C. For vanadium concentrations higher than 30 at %, the Curie temperature of alloys depends on the cooling rate, and for the quenched alloys is higher than for the unquenched alloys [2].

The magnetic behaviour of the σ — phase solid solutions yet is not clear enough So, the 47 6 at. % V alloy become ferromagnetic bellow 203 K, while the 60 at % V alloy is not ferromagnetic even bellow 4 3 K [3]. For the high vanadium concentrated solid solutions the results reported in [3] are much different from those reported in [4, 5].

Experimental. The samples were prepared by arc melting in pure argon atmosphere from high purity metals The melted samples were annealed at 900°C for 336 hours in vacuum of 10^{-6} Torr.

The magnetic susceptibility was measured, using a Weiss-Forrer equipment with 10^{-8} cm^3/g sensitivity [7], in the temperature range 100 — 1200 K and magnetic field intensity of 4,820 Oe. The samples concentration is given in Table 1, and the order number is written on the temperature dependence curves of the reciprocal magnetic susceptibility (Figs 1 and 2)

From the seven investigated samples five are α — solid solutions and two are σ — solid solutions, i e 46 at % V and 55 at % V

Results and discussions. As it is well known, the pur vanadium metals is a Pauli paramagnet type with a quadratic temperature lowering of the magnetic susceptibility [6]. Nevertheless, in some intermetallic compounds and alloys

* *University of Cluj-Napoca, Department of Physics, 3400 Cluj-Napoca, Romania*

vanadium has partial or whole localized magnetic moment [6, 7, 8]. From this point of view, the magnetic behaviour of the vanadium alloys and intermetallic compounds with simple or transition elements may be very different, depending on the heat treatment, or on the crystalline structure

In our case, when the iron concentration increases in the vanadium solid solutions, the magnetic suceptibility also increases, as one can see from the Fig 1.

For the solid solutions with the vanadium concentration 91 ; 88 and 79 at. % V, the magnetic susceptibility is practically temperature independent, i e. this alloys are Pauli paramagnets.

For the less vanadium concentrated solid solutions (72 at % V, 68 at % V etc.), the magnetic susceptibility become temperature dependent, and the reciprocal magnetic susceptibility as function of temperature is not linear (see Fig 1). This means that the observed paramagnetism for these samples is a paramagnetism of localized magnetic moments, for both α and σ — solid solutions. The general aspect of the curves $1/\chi(T)$ suggests that the temperature dependence of the magnetic susceptibility may be described by the Néel low for the paramagnetic state of the ferrimagnetic ordered materials,

$$\frac{1}{\chi} = \frac{1}{\chi_0} + \frac{T}{C} - \frac{\sigma}{T - \sigma}, \qquad (1)$$

where $\frac{1}{\chi_0}$, θ, σ, are the constants depending on the molecular field coefficients, and C is the Curie—Weiss constant, correlated with the atomic effectiv magnetic moment.

The agreement of the Néel low with the experimental results is marked on the figure by full line. One observes a systematic deviation from the Néel low only at the low temperature part of the curves $\frac{1}{\chi}(T)$, connected with the transition from paramagnetic state to ordered ferrimagnetic state.

For the sample with 46 at. % V, the temperature dependence of the reciprocal magnetic susceptibility, given in the figure 2 has a particular shape. At low temperature the curve $\frac{1}{\chi}(T)$ has a broad minimum, specific for the mixed valence system [9—11]

The numerical values of the Néel law constants are listed in Table 1.

Table 1

Sample number	%at V	C	$\mu_{ef} \cdot \mu_B$	$[f_{Fe}(4 \cdot 2)^2 + f_V(3\,87)^2]^{1/2}$	$\frac{1}{\chi_0} \cdot 10^{-4}$	$\sigma \cdot 10^{-4}$	θ, K
1	91	—	—	—	—	—	—
2	88	—	—	—	—	—	—
3	79	—	—	—	—	—	—
4	72	0 032	4 01	3 96	17 756	306 28	10
5	68	0 0363	3 92	3 97	17 8	1 125	50
6	55	0 0397	4.08	4 02	15 176	1 641	4
7	46	0 0396	4 078	4 053	11.212	2.481	90

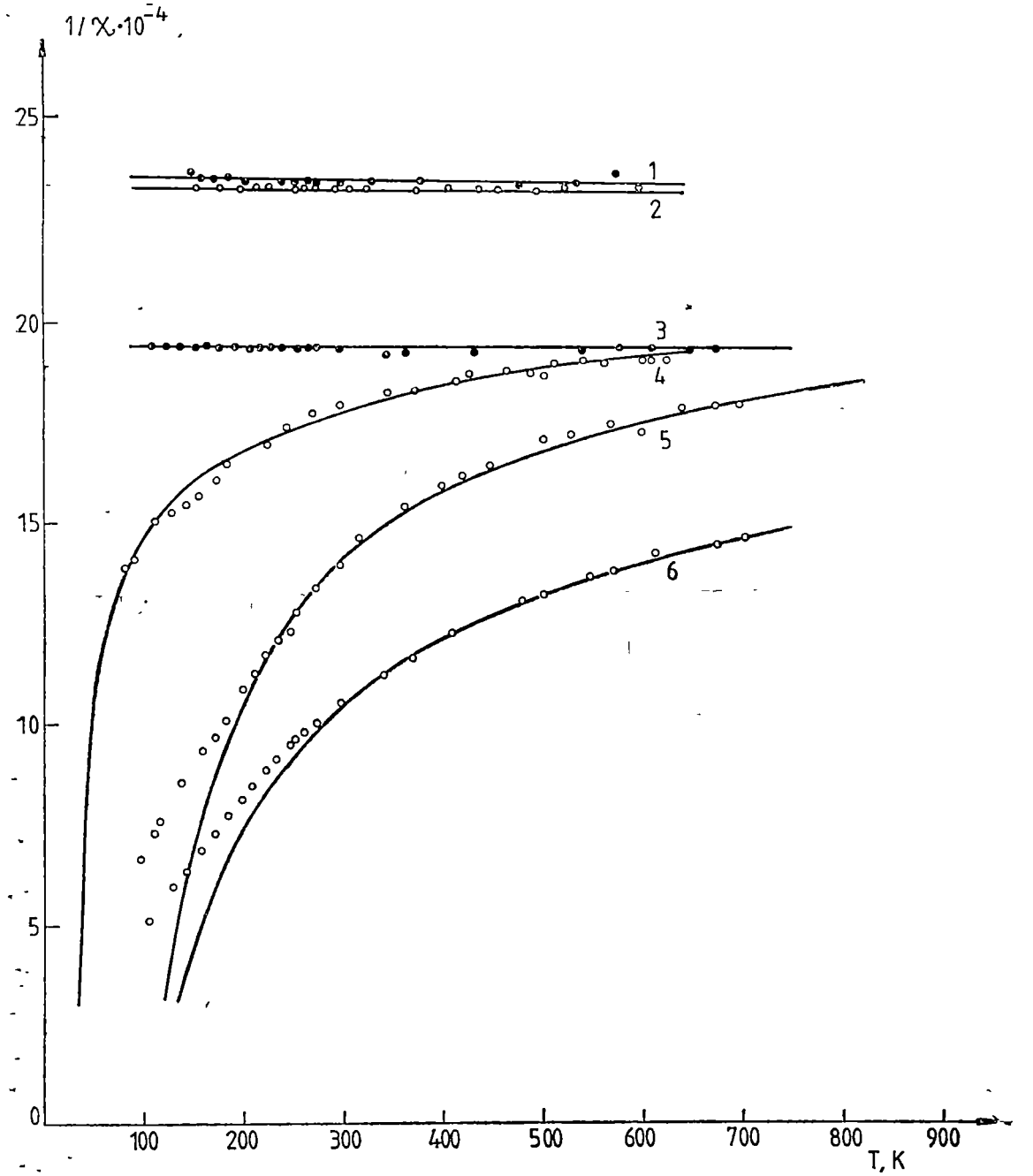
1/χ·10⁻⁴
25
20
15
10
5
0
100
200
300
400
500
600
700
800
900
T, K
1
2
3
4
5
6

Fig 1

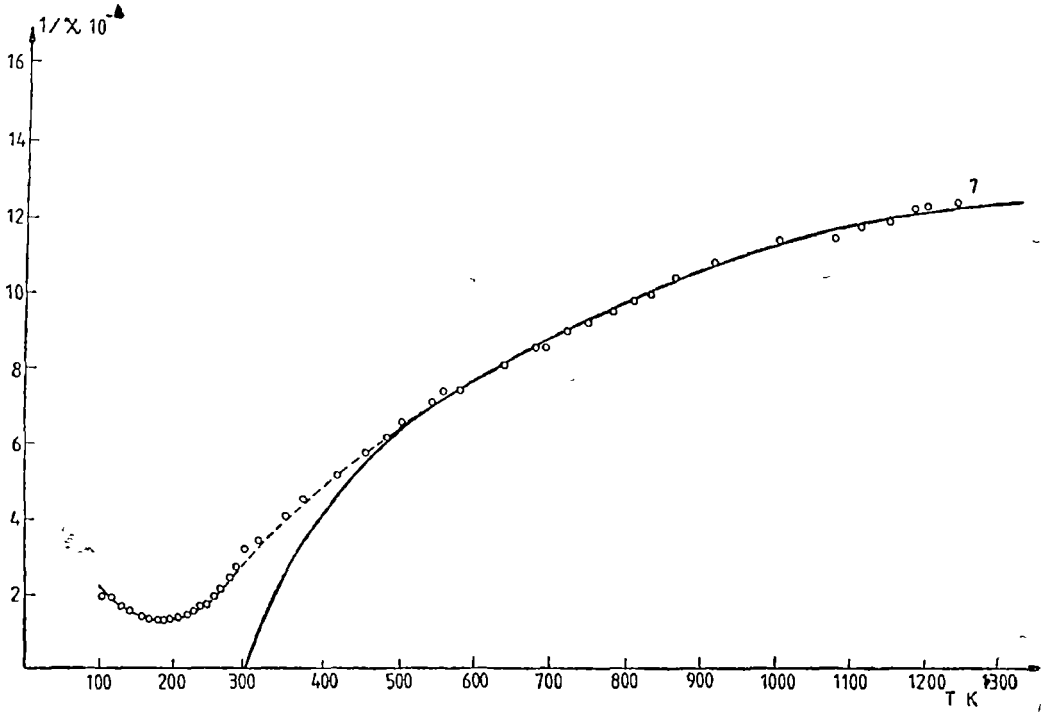

Fig. 2

From the Curie—Weiss constant value we have determined for the last four alloys the effective magnetic moment values, which are in very good agreement with those calculated using the formula

$$\mu_{calc} = [f_{Fe}\,(4\cdot2)^2 + f_V(3.87)^2]^{1/2}, \qquad (2)$$

where f_{Fe} and f_V are the molar fractions for the alloy components. In this formula we have used the whole localized magnetic moment values $4.2\mu_B$/Fe and $3.87\mu_B$/V which correspond per iron atom in pure metallic iron, and per V^{+2} Usually, the vanadium magnetic moment is not localized, but in this case it is really well localized, as it can be see from the values given in Table 1.

Conclusions. The α and σ vanadium-iron solid solutions presents interesting magnetic behaviours. The rich vanadium solid solutions are Pauli paramagnets with temperature independent magnetic susceptibility. The others solid solutions, including σ — solid solutions are ferrimagnetic ordered, withe well localized vanadium magnetic moment, corresponding to V^{+2} ion magnetic moment value. In the σ phase, the solid solution 46 at. % V and 54 at. % Fe exhibit mixed valence characteristic expressed by a broad maximum in the temperature dependence of the magnetic susceptibility at low temperature, perhaps.

REFERENCES

1 M Hansen, K Anderko, „Constitution of binary alloys" (1958)
2 R. M Bozorth, „Ferromagnetizm" (1961)
3. M. V Mevitt and P. A Beck, Trans. AIME, **203,** 669 (1955)
4 N Mori and T Mitui, J Phys Soc Japan, **22, 3,** 931 (1967)
5 N Mori and T Mitui, J Phys. Soc Japan, **26, 5,** 1087 (1969)
6 Iuliu Pop and Marin Coldea, J Magn. Magn Mater, **46,** 81—86 (1984)
7. M. F. Collins and G G. Low, J of Phys, **25,** 596 (1964)
8 S. V. Vonsovski, „Magnetizm", Izd Nauka, Moskva (1971), p 124
9 K Ikeda, K A. Gschneider, Jr, Phys Rev **B 25,** 7 (1982)
10. T. W E Tsang, K A Gschneider, Jr, O. D Mc. Masters, R. J Sterman, S. K Dhar, Phys Rev **B 29,** 7 (1984)
11 T. Tsuchida, W E Wallace, J Chem Phys, **43,** 3811 (1965)

STUDIA UNIV BABEŞ—BOLYAI, PHYSICA, XXXI, 2, 1986

THE USE OF REFLECTANCE INFRARED SPECTROSCOPY FOR THE OBSERVATION OF THE POLYMERIC FILMS ON METALS

S. JITIAN* and I. BRATU**

Received: November 1, 1986

ABSTRACT. — The application of the methods of reflectance infrared spectroscopy for the observation of the polystyrene and poly (methylmethacrylate) films on copper, steel and nickel surfaces is presented. Both specular reflection and internal reflection measurements have been used in order to find the optical constants of the polymeric films. The thickness of the polymeric films on metals has been obtained from the interference fringes in the specular reflectance spectra.

Introduction. The reflection of the radiation on the interface between a medium with refractive index n_0 and an optical absorbing medium with the complex refractive index $\tilde{n} = \bar{n} - i\bar{k}$ are described by Fresnel complex indexes $\tilde{\gamma}_p$ and $\tilde{\gamma}_s$ corresponding to the two components of the radiation that are parallel and respectively perpendicular on the incidence plane:

$$\tilde{\gamma}_p = |\tilde{\gamma}_p| e^{i\delta p} = \frac{\tilde{n} \cos \varphi_0 - n_0 \cos \tilde{\varphi}}{\tilde{n} \cos \varphi_0 + n_0 \cos \tilde{\varphi}} \tag{1}$$

$$\tilde{\gamma}_s = |\tilde{\gamma}_s| e^{i\delta s} = \frac{\tilde{n}_0 \cos \varphi_0 - \tilde{n} \cos \varphi}{\tilde{n}_0 \cos \varphi_0 + \tilde{n} \cos \varphi} \tag{2}$$

where φ_0 is the radiation incidence angle, $\tilde{\varphi}$ is the complex refractive angle, defined by Snellius'refraction law; δ_p and δ_s are the phase differences of the two radiation components after reflection

R_p and R_s reflectances corresponding to the two radiation components, defined as the ratio of the reflected radiation intensity to the incidence radiation intensity, may be expressed allowing for the relationships (1—3) as such:

$$R_p = |\tilde{\gamma}_p|^2 = \left| \frac{(\bar{n} - i\bar{k})^2 \cos \varphi_0 - n_0 \sqrt{(\bar{n} - i\bar{k})^2 - n_0^2 \sin^2 \varphi_0}}{(\bar{n} - i\bar{k})^2 \cos \varphi_0 + n_0 \sqrt{(\bar{n} - i\bar{k})^2 - n_0^2 \sin^2 \varphi_0}} \right|^2 \tag{4}$$

$$R_s = |\tilde{\gamma}_s|^2 = \left| \frac{n_0 \cos \varphi_0 - n_0 \sqrt{(\bar{n}' - i\bar{k})^2 - n_0^2 \sin^2 \varphi_0}}{n_0 \cos \varphi_0 + n_0 \sqrt{(\bar{n} - i\bar{k})^2 - n_0^2 \sin^2 \varphi_0}} \right|^2 \tag{5}$$

We can consider with a good approximation that for the natural unpolarized radiation the reflectance is the arithmetic mean of the two reflectances for both components [1]

$$R = \frac{1}{2} (R_p + R_s) \tag{6}$$

* "Traian Vuia" Polytechnic Institute — I S Hunedoara, 2750 Hunedoara, Romania
** Institute of Isotopic and Molecular Technology, 3400 Cluj-Napoca, Romania

According to these relationships, as a result of the modification with the wavelength of $\bar{n}$ and $\bar{k}$ optical constants of the surface, due to dispersion, the intensity of the reflected radiation changes thus giving the reflection spectrum.

Knowing the reflectances R_p and R_s or R from the reflection spectra, we can compute the optical constants of the reflection surface.

Up to this point both the specular reflectance spectra, when the medium of incidence is the air, and the internal reflectance spectra, may be used when the incidence medium has a greater refractive index than the reflecting surface and the angle of incidence is greater than the limiting angle.

In order to find the two unknown values $\bar{n}$ and $\bar{k}$ we need at least two reflectance measurements It can be measured

— R_p and R_s for the radiation polarized at one angle of incidence;

— R_p and R_s or R_p/R_s for the radiation polarized for two angles of incidence;

— R for the natural radiation for at least two angles of incidence

R and δ can be also measured for the depolarized radiation at a small incidence angle.

The δ value is found from the whole spectrum $R = f(\tilde{\nu})$ based on the Kramers—Kronig integral [2]

In order to find the optical constants from reflectance measurements for at least two incidence angles, graphical methods can be used [3, 4] thus avoiding complicated calculations In this way one can find respectively the optical constants of the metals from the reflection spectra and the optical constants of the polymeric films on metals, from ATR spectra observed for the film covered metal surface

In the case of thin polymeric films the reflection spectrum has a weak resolution This can be improved if the angle of incidence on the polymeric film from a medium with refractive index $n_0 > n_1$ is greater than the limiting angle If the medium on which radiation reflects is optical nonabsorbing, a total reflection is obtained and in the spectra ranges where the medium is absorbing the radiation is partially absorbed so that there will be an attenuated total reflectance spectrum (ATR)

The polymeric film thickness can be determined from the interference fringes in the specular reflection spectra The spectral ranges (2000—2600) cm^{-1} and (3200—5000) cm^{-1} should be used, where most polymers do not produce absorption bands that overlap the interference fringes.

From IR radiation reflection spectra performed at an φ_0 angle of incidence on the polymeric film, assuming that this film is transparent, and with the aid of the refractive index n the film thickness can is calculated by measuring the number of interference fringes N which occur on the spectral range

Because, as in most cases, in the relationship for computing the film thickness

$$d = \frac{N}{2(\tilde{\nu}_1 - \tilde{\nu}_2)\sqrt{n_1^2 - \sin^2 \varphi_0}} \tag{7}$$

the film refractive index value is not always accurately known, we suggest the use of measurements made at two incidence angles φ_{01} and φ_{02}

By measuring the number of fringes N and M in the spectral ranges $\Delta\tilde{\nu}$ and $\Delta\tilde{\nu}'$ from the specular reflectance spectra, recorded at two incidence angle φ_{01} and φ_{02}, the film thickness for each individual case can be found

$$d = \frac{N}{2\Delta\tilde{\nu}\sqrt{n^2 - \sin^2\varphi_{01}}}, \qquad d = \frac{M}{2\Delta\tilde{\nu}'\sqrt{n^2 - \sin^2\varphi_{02}}} \tag{8}$$

Because the measurements are made in spectral ranges which partly overlap each other, we consider that the film thickness and refractive index are the same for both measurements By eliminating the refractive index between the two relationships (8) we obtain the fim thickness

$$d = \frac{1}{2\Delta\tilde{\nu}\Delta\tilde{\nu}'}\sqrt{\frac{M^2\Delta\tilde{\nu}^2 - N^2\Delta\tilde{\nu}'^2}{\sin^2\varphi_{01} - \sin^2\varphi_{02}}} \tag{9}$$

The relationships (8) can also be used to find the average value of the film refractive index on the common $\Delta\tilde{\nu}$ and $\Delta\tilde{\nu}'$ spectral range. By eliminating the film thickness between relationships, (8) and (9) we obtain the refractive index as

$$n = \sqrt{\frac{M^2\Delta\tilde{\nu}^2\sin^2\varphi_{01} - N^2\Delta\tilde{\nu}'^2\sin\varphi_{02}}{M^2\Delta\tilde{\nu}^2 - N^2\Delta\tilde{\nu}'^2}} \tag{10}$$

Experimental. The copper, nickel and OLC 45 steel samples on which polymeric films have been deposed, have been cut from bulk metal to the dimensions of 45 × 22 × 5 (mm) and then ground and polished with abrasive paper up to 12 grain The surface has been further polished with No 2 „Presi" Italia metallographic paper

The sample was washed in water and absolute ethyl alcohol The (PS) polystirene and (PMMA) poly(methylmethacrylate) films were deposited from the polymeric solutions in benzene and trichloromethane during spinning the samples, under conditions similar to those reported by other authors [5, 6]

The IR reflection spectra have been recorded with UR-20 (Carl Zeiss Jena) spectrophotometer in natural light In order to record the specular reflection spectra we used the specular reflectance attachement for 20° and 55° incidence angles

ATR spectra at 45° and 55° incidence angles have been obtained with ATR unit KRS-5-crystal

Results and discussions. The reflection spectra can be used to identify the polymer on a metallic surface due to the resemblence with the transmission polymer spectra The reflection spectrum of the polymer film on the metal can be considered like a transmission spectrum because the radiation IR crosses the polymer film twice as a result of the reflection on the metal surface The ATR polymer films spectra although they are not real absorption spectra ressemble very much with the transmission spectra if they are registered in certain conditions [4].

We used the graphical method in order to determine the metal optical constants We plotted on the same graphic the reflectivity variation curves as the absorption coefficient $\bar{k}$ in accordance with the relations (4—6) for different values of the refractive index $\bar{n}$ The curves family $R = f(\bar{k})$ obtained for the incidence angle of 55° is presented in figure 1. These curves have been plotted on the basis of the values given by Vasiček [3] From this plot the

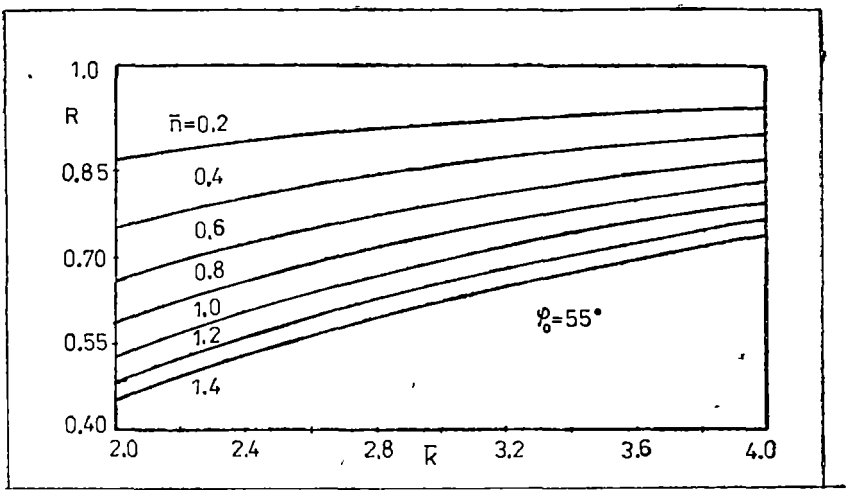

Fig 1. The reflectivity variation curves depending on the absorbtion coefficient for different values of the refractive index $\bar{n}$ at the incidence of 55°.

pairs of values $\bar{n}$ and $\bar{k}$ corresponding to the reflectivity value from the reflection spectrum for the respective incidence angles are obtained. The same way is used for the pairs measurement performed at the incidence angle of 20°. Then, the two pairs of curves $\bar{n} = f(\bar{k})$ are represented on the same graph, like in figure 2. The cross point of the two curves has as coordinates the two optical constants of the surface $\bar{n}$ and $\bar{k}$ corresponding simultaneously to the pairs of values of the reflectivity measured at the two incidence angles. The complex refractive indices of the metals determined in this way in the range IR at 2200 cm^{-1} are:

$\tilde{n} = 1.96 - i.8.7$ for copper, $\tilde{n} = 2.16 - i \cdot 5.3$ for nickel and

$\tilde{n} = 2.63 \cdot i.4.8$ for steel OLC — —45. The values obtained are in accordance with those reported in the literature [4].

In the same manner the optical constants of the polymers films from the ATR spectra, obtained in the range IR at 2200 cm^{-1} were determined as follows: $\tilde{n} = 1\,24 - i \cdot 0{,}02$ for the polystyrene film and $\tilde{n} = 1.2 - i \cdot 0.01$ for the methyl polymethacrylate film.

The polymer films thickness was determined with relation (9) by using

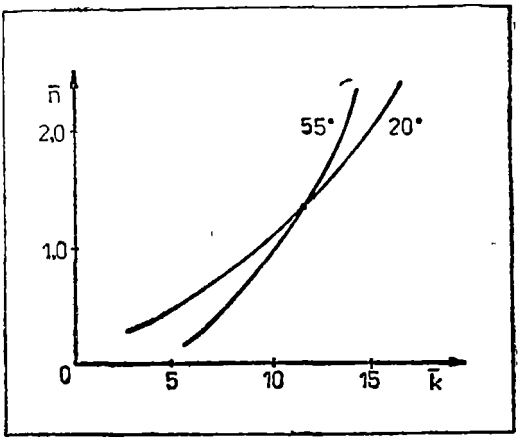

Fig 2 The curves $n = f(\bar{k})$ corresponding to the measured reflectivity for steel OLC 45 at $\tilde{\nu} = 2200\ cm^{-1}$.

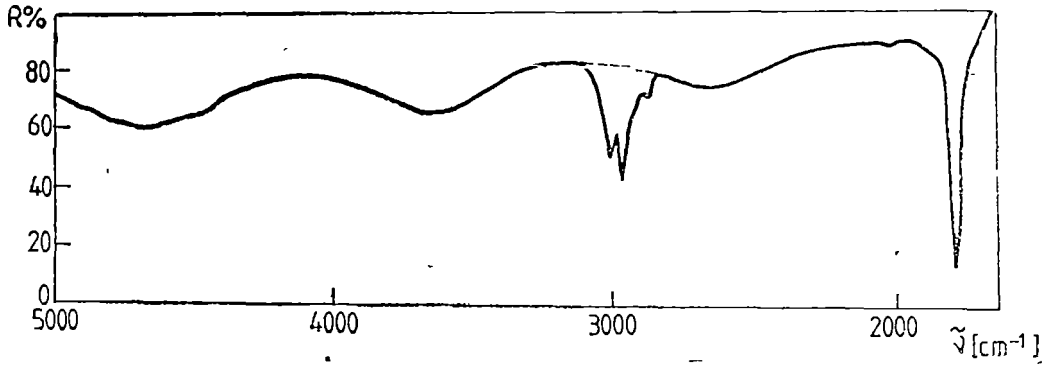

Fig 3 The specular reflection spectrum of the film of PMMA on the steel OLC-45 at the incidence angle of 20°

the reflection spectra of the polymer films on the metals In Fig. 3 the range (1600—5000) cm^{-1} from the specular reflection spectrum of the polymers films of PMMA on OLC—45 steel is presented For the film of PMMA, the film thickness obtained on the basis of the proposed calculus relationship is of 4,2 μm and the refractive index of the film computed with the relation (10) has the value $\bar{n}_1 = 1.15$. The error in calculating the film thickness is of about 0 2 μm if the spectral range between two interference bands is measured with a better accuracy than 50 cm^{-1}. Because the interference bands are measured in the spectral range where the film does not present absorption bands, ($\bar{k}_1 = 0$), in the relations (7—10) only the real part of the film refractive index $\tilde{n}_1 = \bar{n}_1 - i\bar{k}_1$ can be considered.

Conclusions. The IR reflection spectra of the polymer films on the metals are similar to the transmission spectra of the polymers and therefore they can be used for polymer identification on different solid supports.

The optical constants of the metals can be determined in the IR range from the specular reflection spectra at two incidence angles

The polymer film thickness is obtained from the interference bands in the specular reflection spectra of the film on the metal. The calculation of the film thickness, based on two spectroscopic measurements at two incidence angles, avoids the necessity of knowing the film refractive index in the investigated spectral range.

REFERENCES

1 B. Crawford Jr., Th G Goplen, D Swanson, *The Measurement of Optical Constants in the Infrared by Attenuated Total Reflection*, in „Advances in Infrared and Raman Spectroscopy", Chapt 2, vol 4, R J.H Clarck and R E. Hester (Eds), Heyden-London, (1976)
2. G R Wilkinson, *Polarised Infrared and Raman Spectroscopy of Single Crystals*, Chapt. 18, in „Laboratory Methods in Infrared Spectroscopy", R. G. Miller and B. C Stace eds, Leyden —London, p 314, (1972)
3. A Vasiček, „Tables of Determination of Optical Constants from the Intensities of Reflected Light", Nakladatelstvi Ceskoslovenske Akademie Ved, Praga, (1964)
4. G. Kortum, „Reflectance Spectroscopy Principles, Methods, Applications", Springer—Verlag, Berlin, Heidelberg—New York, p 311, (1985)
5 J F Rabolt, M Jurich, J D Swaled, Applied Spectroscopy, **39**, 269, (1985)
6 D. A Saucy, S J Simko, R. W Linton, Analytical Chemistry, **57**, 871, (1985)

STUDIA UNIV BABEŞ—BOLYAI, PHYSICA, XXXI, 2, 1986

IMPURITIES DISTRIBUTIONS IN TOKAMAK PLASMAS

T. A. BEU and M. VASIU

Received November 3, 1986

ABSTRACT — In high temperature low density tokamak plasmas, radiation cooling by impurity atoms an be can important energy loss mechanism [1, 2] since radiation is not reabsorbed The coupled set of time-dependent diffusion equations for ionized impurities is solved in conjunction with a simple model for neutral impurities The resultant density distributions are used in the subsequent computation of the related energy losses Results are presented for oxygen.

Introduction. The ideal magnetically confined fusion plasma would consist only of hydrogen isotopes, helium ions and the neutralizing electrons, well separated from the material walls of the reaction chamber by suitably shaped magnetic fields. In practice, high energy plasma particles leak across the magnetic field, strike the walls and liberate wall material, which diffuses into the plasma, where the impurity atoms (such as carbon, oxygen, iron, nickel, molybdenum) are ionized and excited. Ionization and excitation are accompanied by radiative decay and radiative and dielectronic recombination which lead to unwanted energy losses in addition to the bremsstrahlung radiation. These radiation losses lead to the cooling of the plasma [1, 2].

Eqations. The model adopted for the neutral impurities assumes that these flow into the plasma at thermal velocity V_0 and their density, $n_0(r)$, decreases rapidly through ionization as the impurities penetrate the plasma. Using the coordinates indicated in Fig. 1 we have

$$n_0(r) = \frac{n_0^+}{4\pi} \int_0^{2\pi} d\varphi \int_{-\pi/2}^{\pi/2} d\psi \cos\psi \exp\left[-\frac{1}{V_0} \int_0^{\rho_s} \alpha_1(\rho') n_e(\rho') d\rho' \right] \tag{1}$$

where n_0^+ is the average number of neutrals leaving the unit area of the walls. MKS units are used throughout the paper, except where specifically mentioned. α_1 is the ionization rate for the neutrals and n_e is the electron density. V_0 is approximately given by the following expression

$$V_0 = 4 \times 10^{-10} (T_0/m_z)^{1/2}$$

where T_0 is the temperature of the neutrals in eV and m_z is the mass of the impurity.

The density distributions of the ionized impurities are calculated by taking into account classical and anomalous diffusion and the ionization-recombination

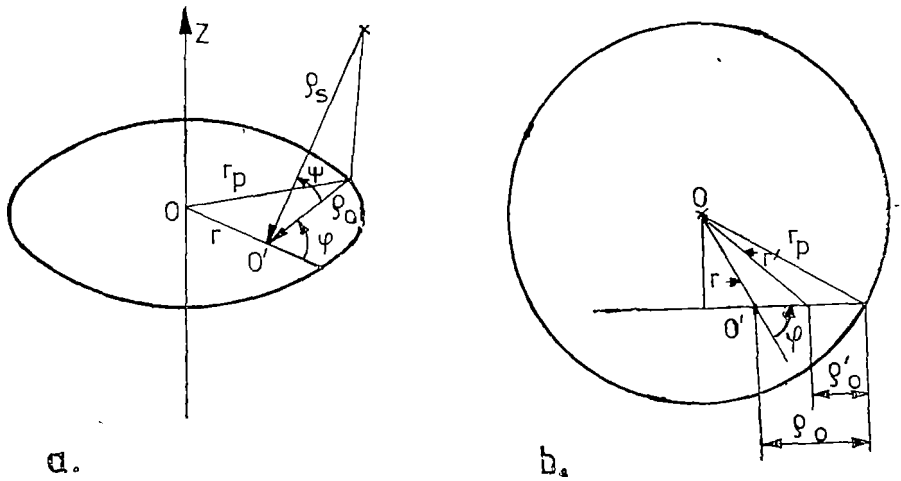

Fig 1 Coordinates employed in the model for neutral impurities

process The radial density distributions are then given by the following set of coupled differential equations:

$$\frac{\partial n_k}{\partial t} + \frac{1}{r}\frac{\partial}{\partial r}(r\Phi_k) - n_e[(1-\delta_{k,1})\alpha_k n_{k-1} - (\alpha_{k+1}+\beta_k)n_k + \beta_{k+1}n_{k+1}] = \delta_{k,1}n_e\alpha_1 n_0 \tag{2}$$

$$k = 1, 2, \ldots, NST,$$

where n_k is the impurity ion density in the k th ionization state, α_k is the ionization rate for the passage from the $(k-1)$ th state to the k th state and β_k is the total recombination rate for the passage from the k th state to the $(k-1)$ th state. NST represents the total number of ionization states and δ is Kronecker's symbol.

The flux of the impurity ions in the k th ionization state is given [4, 5] as

$$\Phi_k = -\gamma_D D_k \partial n_k/\partial r + \gamma_W W_k n_k \tag{3}$$

on the assumption that the impurity ion density is low enough for the effect of mutual collisions to be neglected. The Pfirsch—Schluter diffusion coefficient D_k and the inward diffusion velocity due to friction with plasma ions W_k are, respectively, given by

$$D_k = (1+q^2)\rho_k^2\nu_k \tag{4}$$

$$W_k = kD_k\left\{\frac{1}{n_i}\frac{dn_i}{dr} - \frac{1}{2T_i}\frac{dT_i}{dr}\right\}, \tag{5}$$

where γ_D and γ_W are the anomalous factors. The safety factor q, the Larmor radius ρ_k and the collision frequency of impurity ions with plasma ions ν_k, are defined as follows:

$$q = \frac{r}{R_t}\frac{B_t}{B_p}$$

$$\rho_k^2 = 6\,25 \times 10^{18}\frac{m_z}{B_t^2}\frac{T_k}{k^2}$$

$$\nu_k = 2\,765 \times 10^{-27} n_i (m_i)^{1/2} k^2 \ln \Lambda_k / (m_z T_i^{3/2})$$

Here R_t is the major radius of the reaction chamber, B_t and B_p are the toroidal and the poloidal magnetic fields, respectively, n_i is the plasma ion density, $\ln \Lambda_k$ is the Coulomb logarithm, T_i is the plasma ion temperature and T_k is the impurity ion temperature in eV The effective ionic charge of the plasma is defined as follows

$$\bar{Z} = \left(n_i + \sum_{k=1}^{NST} k^2 n_k\right)/n_e$$

and according to charge neutrality

$$n_i = n_e - \sum_{k=1}^{NST} k n_k$$

The diffusion coefficients depend on the impurity ion temperature T_k, for which we use a simple model:

$$T_k = \begin{cases} \text{const} \quad (k = 0) \\ T_i \text{ for } \tau_{eq} \leqslant t, \ (k \neq 0) \\ \min\,[T_i,\ T_{k-1} + (T_i - T_{k-1})\tau_i/\tau_{eq}] \text{ for } \tau_{eq} > \tau_i (k \neq 0), \end{cases}$$

where $\tau_i = 1/(\alpha_{k+1} + \beta_k) n_e$ and $\tau_{eq} = 1/2\nu_k$. We used the ionization rates given by Lotz [6]

$$\alpha_k = 67 \sum_{k=1}^{NSS} \frac{a_i^k q_i^k}{T_e^{3/2}} \left[\frac{1}{P_i^k/T_e} E_1\left(\frac{P_i^k}{T_e}\right) - \frac{b_i^k \exp(c_i^k)}{P_i^k/T_e + c_i^k} E_1\left(\frac{P_i^k}{T_e} + c_i^k\right)\right]$$

where

$$E_1(x) = \int_x^\infty \exp(-y)/y]dy$$

is the exponential integral, P_i^k is the binding energy of the electrons in the i th subshell (in eV), q_i^k is the number of equivalent electrons in this subshell and a_i^k, b_i^k and c_i^k are fitting constants tabulated in ref. [6] NSS stands for the number of subshells considered

Taking into account the radiative recombination rate [8] and the dielectronic recombination rate [9], the approximate expression for the total recombination rate is $\beta_k = \beta_k^r + \beta_k^d$

Equations (2) are solved under the following boundary conditions:

$$[n_0(r)]_{r=r_p} = \text{given constant}$$

$$[n_k(r)]_{r=r_p} = 0, \quad k = 1, 2, \ldots, NST,$$

$$\left[\frac{\partial n_k}{\partial r}\right]_{r=0} = 0, \quad k = 1, 2, \ldots, NST$$

and in considering the time-dependent cases one adds the initial conditions

$$n_k^{t=0}(r) = n_k^0(r), \quad k = 1, 2, \ldots, NST$$

The energy losses by ionization, recombination, bremsstrahlung and excitation due to the presence of the impurities are approximately given by

$$p_i = 1\,6 \times 10^{-19} \sum_{k=1}^{NST} n_e n_{k-1} \alpha_k \left(P_1^k + \frac{3}{2} T_e\right) + p_{rec}$$

$$p_{rec} = 1\,6 \times 10^{-19} \sum_{k=1}^{NST} \frac{3}{2} n_e n_k \beta_k T_e,$$

$$P_{br} = 1\,5 \times 10^{-38} \bar{Z} n_e^2 T_e^{1/2}$$

$$P_{ex} = 1\,73 \times 10^{-31} T_e^{-1/2} n_e \sum_{k=1}^{NST-1} n_k \sum_{l=1}^{L} c_{kl} \exp\left(-\frac{P_{ex}}{T_e}\right)$$

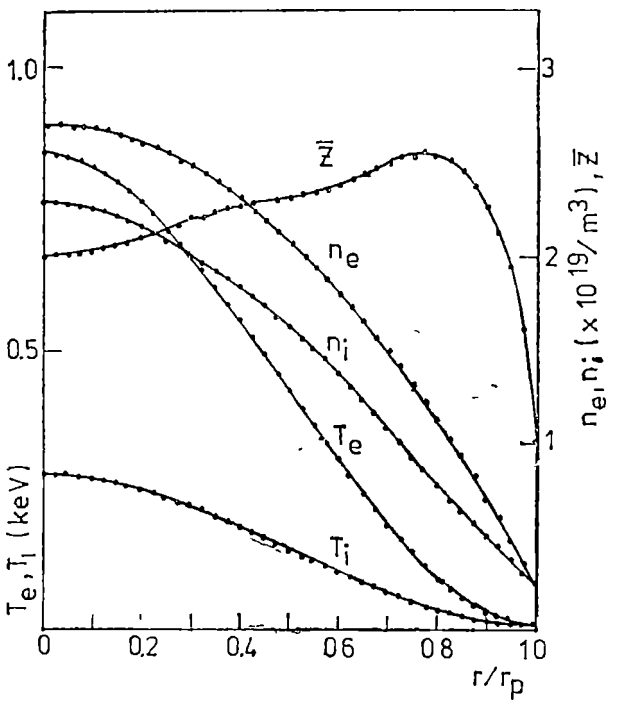

Fig 2 Input profiles for n_e, T_e and T_i, output profiles for n_z and $\bar{Z}$

where P_{ex} is the excitation potential. The coefficients c_{kl} are tabulated in ref. [5].

Equations (2) were approximated by simple finite difference schemes

Results. Calculations were made for oxygen impurity ions. Fig 2 presents our input profiles for the electron density n_e, electron temperature T_e, plasma ion temperature T_i and the output profiles for plasma ion density n_i and for effective ionic charge $\bar{Z}$ Our input data correspond to a typical experiment in the hydrogen plasma of the ST tokamak.

Fig 3 shows the resulting impurity density profiles The figures attached to each curve denote the ionization state of the impurity (the neutrals are labeled with 0, the simple ionized oxygen with 1, etc) Fig 4 gives the radiative energy losses obtained with the impurity density profiles of Fig 3. Our results seem to agree fairly with those of Tazima et al. [5].

The algorithm and the program based on it have been presented in a previous paper [10]

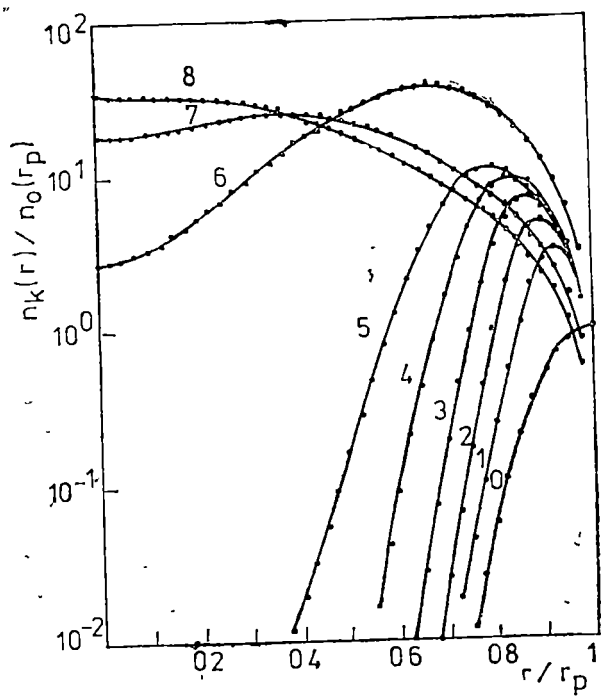

Fig 3 Output oxygen impurity density profiles.

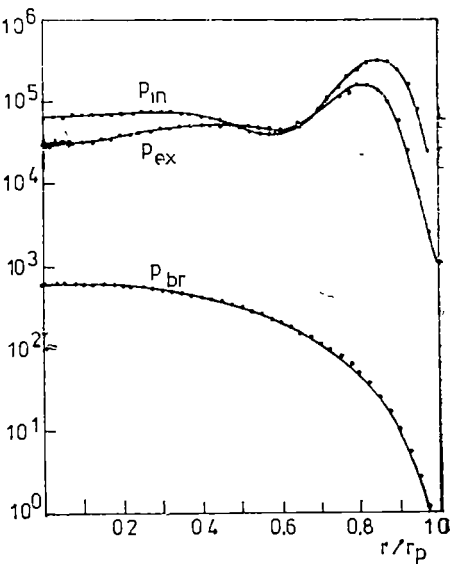

Fig 4 Radiative energy losses obtained with the impurity density profiles of fig 3

REFERENCES

1. H. W Drawin, Phys Rep 37 (1978) 125
2. H W. Drawin, Phys Scripta 24 (1981) 622
3. W G Bickley and J Nayler, Phil Mag 20 (1935) 343.
4 A. Samain, EUR—CEA—FC—745 (1974)
5 T. Tazima *et al*, Nucl Fusion 17 (1977) 419
6. W Lotz, IPP 1/62 (1967)
7 K. L Bell *et al.*, Report CLM—R 216 (1982)
8 S. von Goeler *et al*, Nucl Fusion 15 (1975) 301.
9. EUR—CEA, MAKOKOT — Code d'evolution (August 1977)
10 T. A. Beu *et al*, Comput Phys. Commun 36 (1985) 161.

STUDIA UNIV BABEŞ—BOLYAI, PHYSICA, XXXI, 2, 1986

ESR AND THERMAL ANNEALING STUDIES OF γ-DEFFECTS IN Na_2SeO_4

I. BARBUR* and L. STĂNESCU*

Received November 6 1986

ABSTRACT. — ESR study of γ-irradiated Na_2SeO_4 in powder form indicates the existence of SeO_2^-, SeO_3^- and SeO_4^- radicals The identification of radicals is made on the basis of their g tensors The radical SeO_4^- appears in ESR spectra at 77 K only The activation energies involved in process of recombination of SeO_2^- and SeO_3^- radicals are evaluated

Introduction. Sodium selenate belongs to a large class of substance as $NaNH_4SeO_4$, K_2SeO_4, wich presents ferroelectric transition [1—2]

This paper presents ESR investigations of γ-irradiated powder of sodium selenate Na_2SeO_4, at both room temperature and 77K The study of the thermal annealing of deffects produced by gamma irradiation in Na_2SeO_4 in the range of temperature from 60°C to 170°C is also presented.

Experimental. Paramagnetic centers in Na_2SeO_4 were produced by γ-irradiation of the samples to a ^{60}Co source for 100 hours

Electron spin resonance (ESR) spectra were recorded by a JES-3B type spectrometer, in the X band, by direct detection using a magnetic field modulation of 100 kHz The temperature in the resonant cavity was controlled using a JES-VT-2 type installation and measured by means of a copper-constantan thermocouple The samples of Na_2SeO_4 were used in powder forms

Results and discussion. Gamma-irradiation of Na_2SeO_4 produces paramagnetic deffects identified as SeO_2^-, SeO_3^-, SeO_4^-. The identification of the species is based on the g-factors and the hiperfine coupling constant of ^{77}Se (I = 1/2).

The ESR spectra of this species in powdered Na_2SeO_4, at 300 K and 77 K are shown in Fig. 1. The values of the g-tensor obtained from analysis of these spectra are given in Table 1

Table 1

g tensor for SeO_2^-, SeO_3^- and SeO_4^- radicals in γ — irradiated Na_2SeO

Radical	T(K)	g		
		g_{xx}	g_{yy}	g_{zz}
SeO_2^-	300	1 9970	2 0272	2 0073
	77	1 9949	2 0260	2 0088
SeO_3^-	300	2 0136	2 0136	2 0025
	77	2 0181	2 0181	2 0015
SeO_4^-	300	—	—	—
	77	(A) g = 1 9660,	(B) g = 2 0356	

* *University of Cluj-Napoca, Department of Physics, 3400 Cluj-Napoca, Romania*

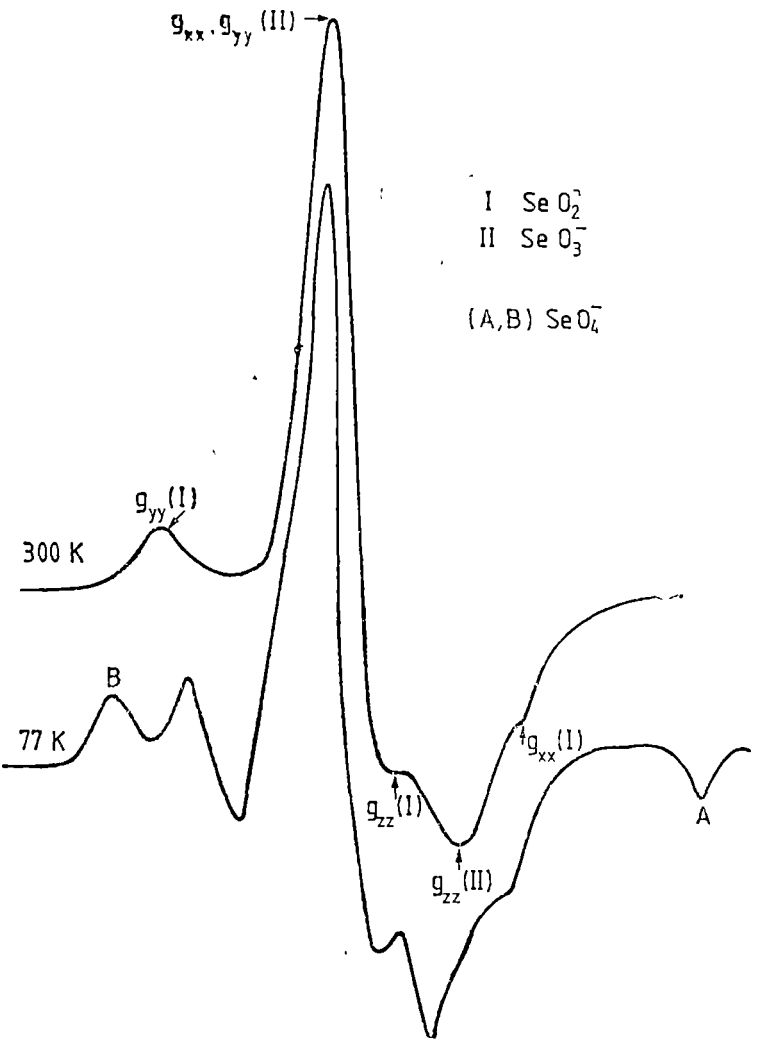

Fig 1 ESR spectrum of powder Na_2SeO_4 at 300 K and 77 K

At room temperature the principal line (II) is atributed to the radical SeO_3^-, which has been detected earlier in K_2SeO_4 [2, 3] and $NaNH_4 \cdot SeO_4 \cdot 2H_2O$ [4]

According to our measurements, the g-tensor is axially symmetric for this radical.

The xial value of the g-tensor $g_{xx} = g_{yy} = 2\,0181$ is greater than for SO_3^- ($g = 2\,0036$) and is atributed to the large value of the spin-orbit coupling constant for selenium [4]

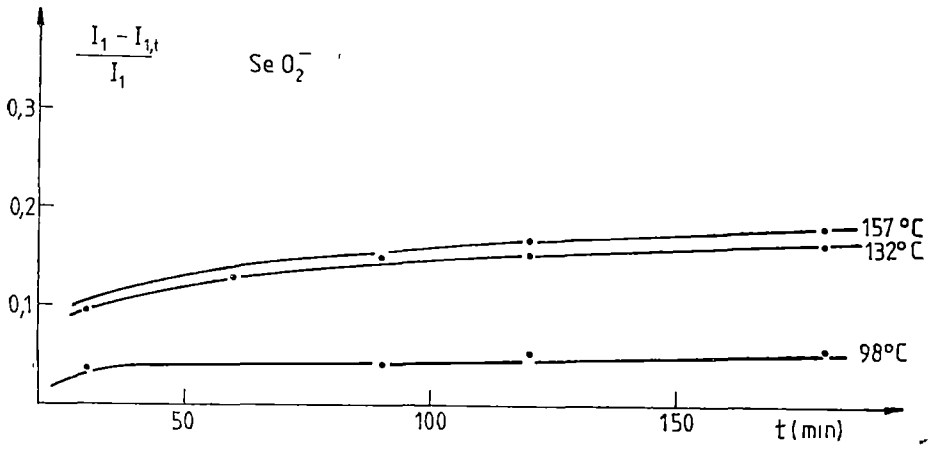

Fig 2 Annealing isoterms for SeO_3^-

/ The radical SeO_2^- has also been observed in a variety of γ-irradiated selenates and selenites [2—4]

The g-tensor for SeO_2^- shows rhombic symmetry and there are not great differences between g-values at the room temperature (300 K) and at the low temperature (77 K).

The radical SeO_4^- was first observed in γ-irradiated K_2SeO_4 at 77 K [2]. The radical disappears by warming the sample up to the room temperature and it has been used as a probe for studying the ferroelectric transition in K_2SeO_4 [3], $NaNH_4SeO_4 \cdot 2H_2O$ [5] The ESR spectrum of SeO_4^-, at room temperature, is masked by the radicals SeO_2^- and SeO_3^- According to our measurements (Fig 1), two rhombic components A and B of the radical SeO_4^- are observed at low temperature (77 K) The g-values of these components (Table 1) are in good agreement with the same values observed for SeO_4^- in $NaNH_4 \cdot SeO_4 \cdot 2H_2O$ [4]

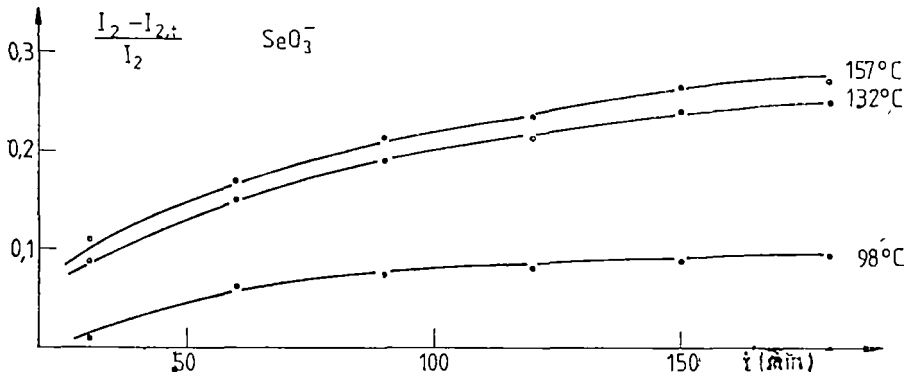

Fig 3 Annealing isoterm for SeO_3^-

The temperature stability of the radicals SeO_2^- and SeO_3^- was studied in the temperature range from 60°C to 160°C by measuring the variation of the ESR signal (amplitude of the line) at different temperatures In Fig 2, the value $I_1 - I_{1,t}/I_1$ is plotted against time, where I_1 is the initial amplitude of the component for SeO_2^- and $I_{1,t}$ is the amplitude after t minutes of heating. Figure 3 represents the annealing isoterms for SeO_3^-.

No changes in the intensity of the ESR lines were observed for both SeO_2^- and SeO_3^- radicals, below 98°C

By increasing the temperature, a continuous decrease of the signal is observed corresponding to the recombination process of the radicals

The activation energies in the recombination process of SeO_2^- and SeO_3^- radicals were calculated using a phenomenological method [6] and are 0 265 eV for SeO_2^- and 0.195 eV for SeO_3^-.

By investigation of the structural changes which appear in Na_2SeO_4 at the transition point evidenced by the properties of the SeO_4^- radical, the studies of the possible incommensurate state in Na_2SeO_4 are in progress

REFERENCES

1 Aleksandrov, K S, Aleksandrova, I P, Zherebtsova, L I, Zaitseva M P, Anistratov A T, Ferroelectrics **2**, 1 (1971)
2 Atkins, P W., Symons, M C R, Wardale, H W, J Chem Soc, **5**. 5215 (1964)
3 Aiki, K, J Phys Soc Japan, **29**. 379 (1970)
4 Ramani, K, Srinivasan, R, *Mol Phys*, *44*, 125 (1981)
5 Ramani, K, Srinivasan, R, Proc Nucl and Solid State Phys Symp, (DAE), Bangalore, C, **16**, 367 (1973)
6. Căluşaru, A, Barbur, I, Ursu, I, „Chemical Effects of Nuclear Transformation", Vol. II, IAEA, Vienna, 239—313 (1965)

STUDIA UNIV BABEŞ—BOLYAI, PHYSICA, XXXI, 2, 1986

MAGNETIC PROPERTIES OF COBALT CADMIUM—BORATE OXIDE GLASSES

I. ARDELEAN*, GH. ILONCA*, O. COZAR* and V. SEVIANU*

Received November 12, 1986

ABSTRACT. — The results of magnetic investigations on $xCoO(1-x)$ $[2B_2O_3\ CdO]$ glasses with $0 < x \leqslant 50$ mol % are reported These show that the cobalt ions, are in bivalent state The atomic magnetic moments of Co^{2+} ions decrease from a value of 5 173 μ_B for the 3 mol % CoO to a value of 3.893 μ_B for 50 mol % CoO. These variation can be attributed to a statistical average of the cobalt distribution states. The magnetic susceptibility data suggest the appearance of the magnetic superexchange interactions for $x \geqslant 5$ mol %.

Introduction. Juza *et al.* [1] reported magnetic investigations on a series of cobalt alkali-borate glasses by varying the alkali-metal oxide (Na_2O, Li_2O) content If has been determined that the atomic magnetic moment of Co^{2+} ion decreases when the alkali-metal oxide concentration increases The decrease in the magnetic moment takes place at about the same content of the alkali-metal oxide at which the colour of the glass changes. Verhelst *et al* [2] have reported that the cobalt aluminosilicate glasses show Curie—Weiss behaviour with large negative paramagnetic Curie temperatures and reveal a very noticeable trend in the magnitude of the atomic magnetic moments as a function of composition. We have investigated the cobalt in lead-borate [3] and potassium-borate [4] oxide glasses, keeping the B_2O_3/PbO and B_2O_3/K_2O ratio constant In these glasses, the cobalt ions are in bivalent state, having the atomic magnetic moments constant in agreement with those obtained by Egami *et al* [5] for cobalt phosphate oxide glasses.

Experimental. In order to obtain further information on the magnetic behaviour of cobalt ions in oxide glasses, we have investigated the $x\,CoO\,(1-x)$ $[2B_2O_3 \cdot CdO]$ glasses, with $0 < x \leqslant 50$ mol % Initially the glass matrix $2B_2O_3 \cdot CdO$ was prepared by mixing H_3BO_3 and $CdCO_2$ and then melting this admixture in a sintered corundum crucible, using the technique previously reported [3, 4] After cooling, the glass matrix was crushed and resulting powder mixed with CoO before final melting at T = 1200 °C for 1 h The structure studied by X-ray analysis did not reveal any crystalline phase up to 50 mol % CoO

The magnetic measurements were made between 80 K and 320 K, using a Faraday type balance

Results and discussions. The temperature dependence of the reciprocal magnetic susceptibility of the various glasses is presented in Fig. 1. For the glasses with a CoO content $\leqslant 3$ mol % the Curie law is observed. This suggests that up to 3 mol % in these glasses, the cobalt ions are magnetically isolated. For a CoO content higher than 3 mol %, the reciprocal magnetic susceptibility obeys a Curie—Weiss behaviour, with a negative paramagnetic Curie tempera-

* *University of Cluj-Napoca, Department of Physics, 3400 Cluj-Napoca, Romania*

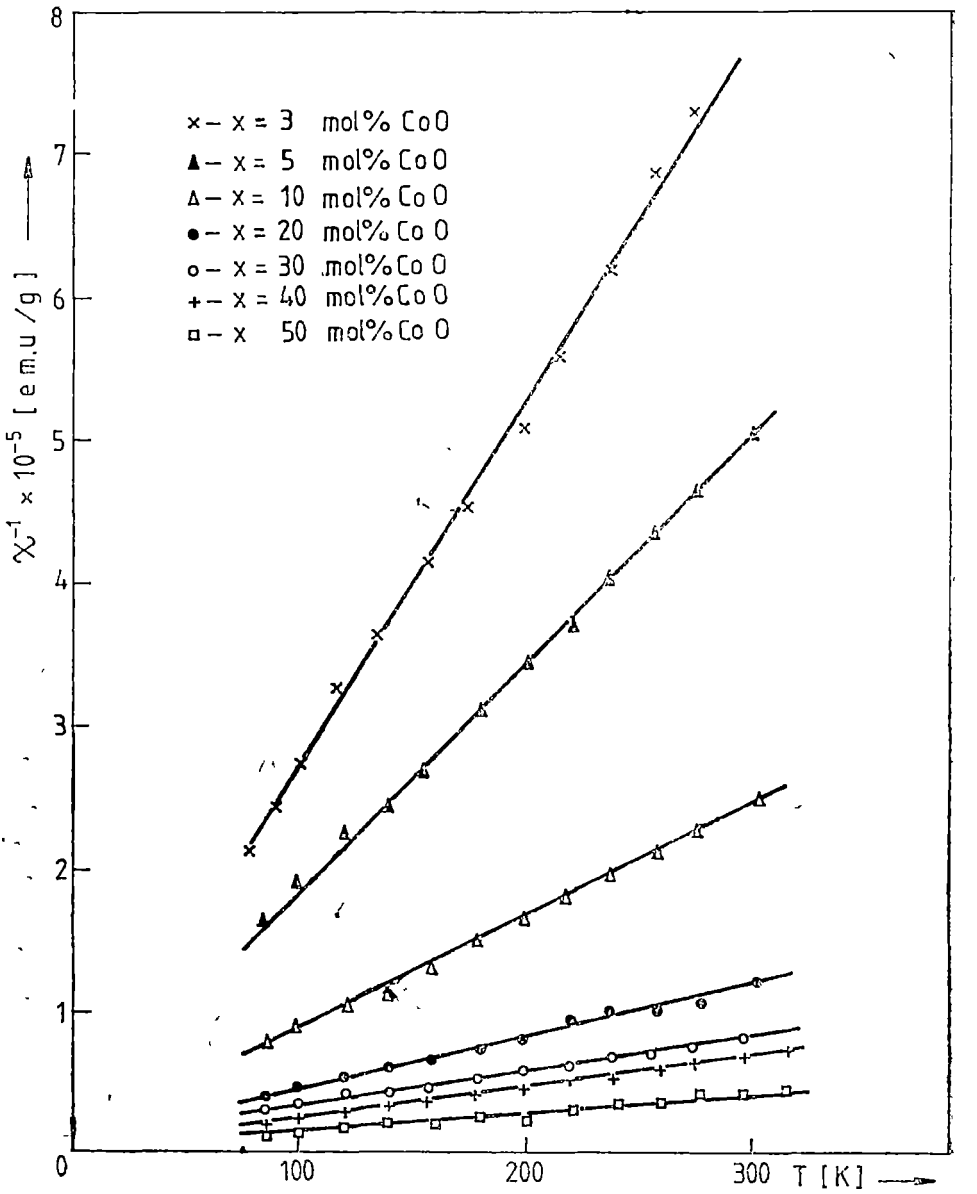

Fig 1 Temperature dependence of the reciprocal magnetic susceptibility.

ture For these compositions, the high temperature susceptibility data indicate that the cobalt ions in the glasses undergo negative exchange interactions and are coupled antiferromagnetically The antiferromagnetic order is formed at a short range only and may be described by the so-called micromagnetic type order [4] A similar conclusion was reached for Co^{2+} ions in aluminosilicate [2] and potassium-borate [4] oxide glasses

The composition dependence of the paramagnetic Curie temperature, θp, is presented in Fig 2. The absolute magnitude of the values of θp increases almost linearly for $x > 3$ mol % In general, the exchange integral increases together with the concentration of the transition metal ions in the glass [6] This reflects a gradual increase in the magnetic interactions in the system and is due to the increasing of the number of cobalt ions which are participating in these interactions.

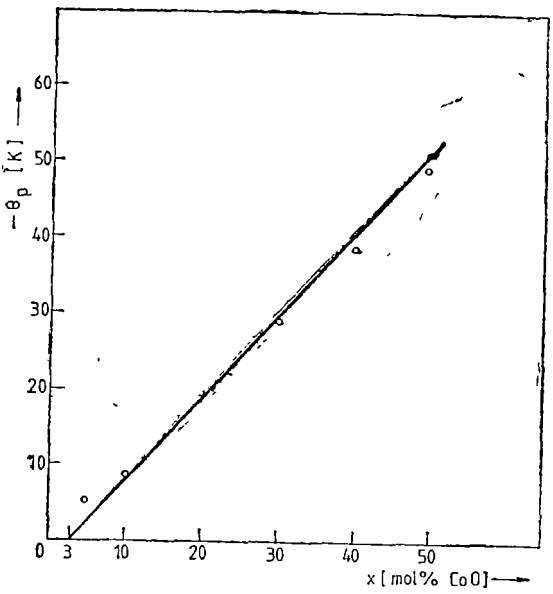

Fig 2 Composition dependence of the paramagnetic Curie temperature

To determine accurately the values of the Curie constants, C_M, and atomic magnetic moments, μ_{at}, corrections due to the diamagnetism of the glass matrix and CoO were taken into account. The composition dependence of the Curie constants, C_M, and of the atomic magnetic moments, μ_{at}, are presented in Figs. 3 and 4. For the glasses with $x > 5$ mol %, the experimental values obtained for Curie constant, which are proportional to the ion concentration, increase with cobalt ion concentrations but less rapidly (Fig. 3).

The experimental values obtained for the atomic magnetic moments, μ_{at}, therefore decrease from value of 5.173 μ_B for 3 mol % CoO to a value of 3.893 μ for the 50 mol % CoO (Fig. 4). A similar conclusion was reached by Verhelst *et al* [2] in their study of Co^{2+} in aluminosilicate glasses. These values are higher that the values of the magnetic moment of Co^{2+} ions in free ion state: $\mu_{0}^{Co^{2+}} = 3.87\ \mu_B$ when only the spin moment is active. When, in addition, there is full orbital contribution, we have $\mu = g_J\sqrt{J(J+1)} = 6.63\mu_B$, with $g_J = 1.33$ for Co^{2+} ion with electron configuration $3d^7$ in $^4F_{9/2}$ ground state [7]. The experimental values for high-spin Co^{2+} complexes lie between 4.4 μ_B and 5 2 μ_B [8].

Our results suggest that the cobalt ions exist in divalent state in $2B_2O_3 \cdot CdO$ glasses, as was also observed in alkali-borate [1] phosphate [5] and aluminosilicate [2] oxide glasses.

It can be shown from the energy level diagram of Co^{2+} ion [1] that a lower magnetic moment is to be expected for the octahedral coordination (*A*

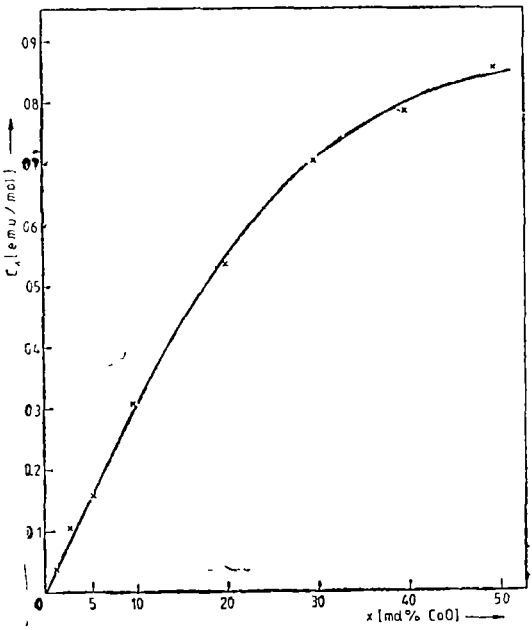

Fig 3 Composition dependence of the Curie constant.

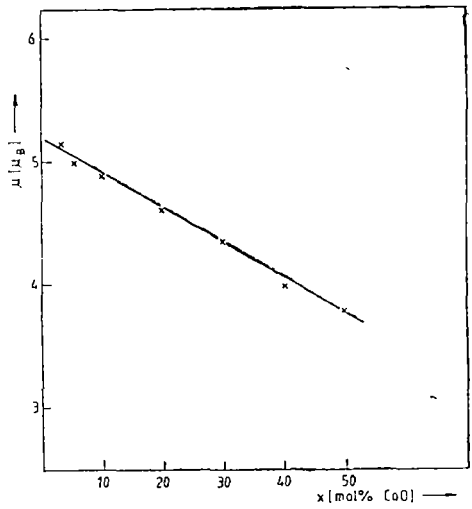

Fig 4 Composition dependence of the atomic magnetic moment

ground state) than for the tetrahedral coordination (T ground state). The observed magnetic moments in our glasses must be the result of a statistical average of the cobalt sites distribution [1]. Thus, at the lower CoO content the tetrahedral coordination prevails, while at the higher those of the octahedral coordination. In the intermediate concentration range a statistical average over these coordination types is present. Similar results have also been evidenced for Ni^{2+} ions in the lead-borate oxide glasses [9]. But we do not exclude the presence of one type of coordination of Co^{2+} ions for which the local distortion varies at different CoO concentrations [10].

It is interesting to remark that in the case of Co^{2+} ions in lead-borate [3] and potassium-borate [4] oxide glasses, the atomic magnetic moment is independent of cobalt ion concentrations.

REFERENCES

1. R Juza, H. Seidel, J. Tiedema, Agew. Chem **78**, 41 (1966)
2. R. A. Verhelst, R. W. Kline, A. M. de Graaf, H. O. Hooper, Phys. Rev. **B 11**, 4427 (1975)
3. I. Ardelean, Gh. Ilonca, D. Bărbos, Solid State Commun., **39**, 1345 (1981)
4. I Ardelean, Gh. Ilonca, N Farkas, C. Lucaciu, M Galffy, Czech J Phys., **B 32**, 1283 (1982)

5 T. Egami, O. S Sacli, A W Simpson, A. L. Terri, „Amorphous Magnetism", (Edited by H O. Hooper and A. M. de Graaf). Plenum Press, New York, 1973, p. 27
6. E J Friebele, N C Koon, L K. Wilson, D. L Kinser, J. Am Ceram Soc. **57**, 237 (1974)
7 E. Burzo, Fizica fenomenelor magnetice, vol 1, Ed Acad RSR, Bucureşti, 1979, p 241
8 L. M. Mulay, „Magnetic susceptibility", Interscience Pbs. New York, 1963, p. 1773
9. I Ardelean, Gh. Ilonca, D Bărbos, H. Adams, Solid State Commun., **40**, 769 (1981)
10 H. G. Hecht, J. Chem Phys., **47**, 1840 (1967)

STUDIA UNIV BABEŞ—BOLYAI, PHYSICA, XXXI, 2, 1986

PbSe FILMS PREPARED BY CHEMICAL DEPOSITION

Al. DARABONT*, P. FITORI*, L. P. BÍRÓ*

Received November 14, 1986

ABSTRACT. — The paper presents a method of growing photoconductive PbSe thin films on glass substrates by chemical deposition, using sodium selenosulfate as selenium ion source, and lead citrate complex The influence of reaction conditions on the film quality is investigated Films obtained using this method are as good as those using selenourea

Introduction. The detection of IR radiation at room temperature in the spectral range of 3—4 μm may be achieved by photoconductors with maximum optical absorption in this range The use of PbSe films as high sensitivity IR detectors in the above mentioned spectral range, in gas-analyser type or other electrooptical devices is but one of the numerous applications which keep up continous scientific and technological interest for these films

For the mentioned spectral range the specialised reference material recommands PbSe films deposited on substrates by one of the following methods: vacuum evaporation, epitaxial deposition or chemical deposition from aqueous solutions (1, 2, 3)

The purpose of this work was to prepare PbSe films in a chemical way by homogenous precipitation on glass substrates from aqueous solutions. The formation of PbSe films from these solutions on a substrate, is determined mainly by the manner of carrying out the chemical reaction between Pb^{2+} and Se^{2-} ions When the reaction is developing slowly enough, the controlled formation of the films takes place This may be accomplished by the severe regulation of component concentrations

In order to stabilize the concentration of Pb^{2+} ions they are taken in the form of stable complexes (as oxalate-, tartarate-, or citrate complex) in an alkaline medium (pH 10—11). There are two basic methods to achieve homogenous precipitations, which differ in the agent that furnishes selenium ions Earlier this used to be selenourea, or its derivatives (4, 5), and later sodium selenosulfate (6)

This latter method was used for the carrying out of the present work. The paper deals with the technology of producing PbSe films by chemical deposition using sodium selenosulfate as a source for selenium ions

II **Experimental details.** II 1 *Preparation of sodium selenosulfate* Sodium selenosulfate solution of a given concentration may be obtained by solving elementary selenium in a sodium sulfite solution [7, 8] The solubility of selenium at a certain temperature is proportional to the concentration of the starting sulfite solution (in the range of 0,2—2 M)

At a constant temperature and at a certain value of pH the ratio of Se/SO_3^{2-} in the solution is constant Higher values of pH increase selenium solubility in the solutions of sulfites

The concentrations of the solutions prepared by us were in the range of 0,05—0,15 M

* *Institute of Isotopic and Molecular Technology, 3400 Cluj-Napoca, Romania*

II.2. *The deposition of PbSe films from solutions containing selenosulfate.* Fofanov and Kitaev (6) have analysed the deposition conditions of different metal selenides from aqueous solutions containing sodium selenosulfate

Using sodium selenosulfate Glistenko (9) et al. obtained mirrorlike films, but the obtaining of any photoconductive films, by this method, was not reported The procedure described in the present paper made it possible to obtain photoconductive PbSe films Some physical properties of these films are reported in (10, 11)

The deposition of PbSe films from aqueous solutions may be achieved after the following diagram

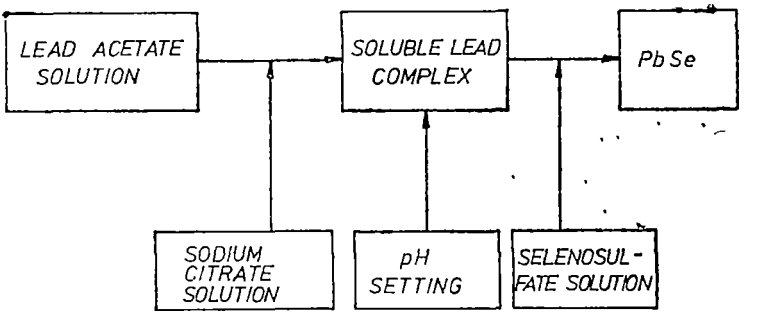

Diagram Technological diagram for PbSe film deposition from aqueous solutions

The concentration of the prepared lead acetate solution was 0,1 M, the same as the concentration of the sodium citrate A lead citrate complex has been prepared by pouring together these two solutions and setting the pH at a chosen value with 1 M ammonia solution The calculated amount of sodium selenosulfate solution was added to the complex, and after mixing, this constituted the deposition bath for the previously cleaned glass substrates.

The growth of PbSe films on the glass substrates has been accomplished in a simple laboratory setup shown in Fig. 1 A laboratory vessel (2) containing the lead complex solution with the value of pH previously set in the range of 9,5—11,5 is placed on a magnetic stirrer (1) with heating facility. The solution is heated to 60—80°C, after which the previously cleaned glass substrates (3) are introduced The 24 × 24 × 0,17 mm substrates are fixed on special supports After the substrates have been introduced the sodium selenosulfate solution is added either continously using the burette (5) or all at once, depending on the experimented variant

The thermostatation of the reaction mixture is used also at lower temperatures and longer reaction times In this case the reaction vessel is placed in the enclosure of an ultrathermostat

A tipical composition of the reaction mixture we used consists of the following amounts of solutions in a vessel of 150 ml.

50 ml lead complex solution
40 ml distilled water

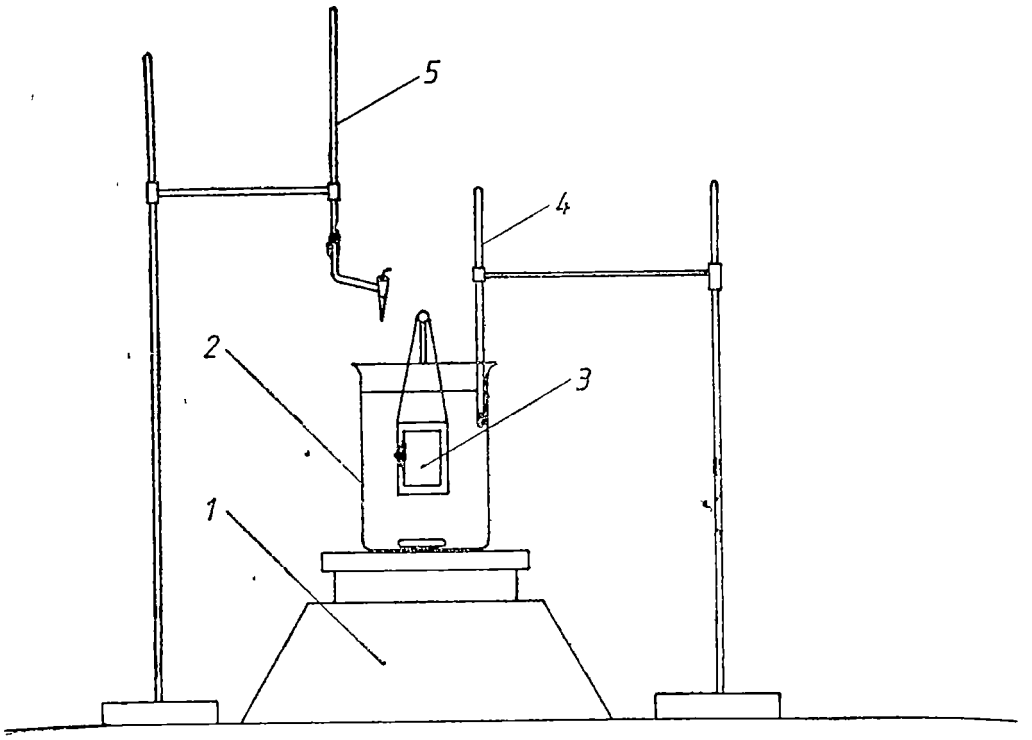

Fig 1 Laboratory setup for chemical deposition of PbSe films on glass substrates

3—5 ml 1 M NH_4OH solution (depending on the chosen pH)
15 ml sodium selenosulfate solution

Deposition time ranges from 5 to 60 minutes When thermostating the reaction mixture at lower temperatures (i.e. 30—40°C) reaction times of several hours were used

III **Results and discussions.** Using the procedure described above, we obtained films with a good quality In order to control deposition technology we have studied the influence of some factors on the quality of the films obtained

— the addition time of sodium selenosulfate solution: at temperatures near 80°C, and pH in the range of 11,0—11,5 reaction speed is relatively high The continuous addition of the selenosulfate solution favourized the formation of adherent and quite thick films When using reaction times up to 60 minutes the thickness of the deposited films ranges from 0,4 μm to 1,6 μm It was found that adding the selenosulfate solution all at once at lower pH values (10—10,5) immediately triggered the process of precipitation even at the temperature of 13°C

— deposition time has a direct influence on the thickness of the films obtained Under identical conditions films of 0,4—0,5 μm were obtained in

30 minutes, while in 60 minutes film thickness reaches the value of 0,9—1,4 μm.

— the pH value of the solution the thickness of the film strongly depends on the pH of the solution It increases with the stronger alkalinity of the solution, but optimum deposition takes place only in the range of 10,5—11,5

— geometrical conditions and the stirring of the solution it was found that the thickness of the films depends on the position of the substrate holder relative to the sense of rotation of the liquid in the vessel. Due to the inclusion of the larger crystallites formed in the volume of the solution, the two faces of the deposited substrate are not identical. The face which is protected from including the crystallites formed in the volume of the liquid is of a better quality.

— the concentration of the reactants in order to control the dimensions of the crystallites forming the deposited film we tried two methods

— the decrease of reactant concentrations

— the use of lower reaction temperatures

In these cases, in order to obtain the same thickness that resulted in the case of undiluted solutions and high reaction temperatures it was necessary to increase deposition time.

— the influence of temperature: at lower temperatures (30—40°C) the reaction would not start easily, deposition is slow, and due to these reasons longer reaction times of the magnitude of several hours must be used to achieve a thickness of 1 μm

— the age of the solutions· it was found that the age of the solutions influences deposition A newly prepared lead complex solution reacts rapidly and produces thinner, mirrorlike films. A few days after having it prepared reaction rate is lower and deposition produces thicker, good quality films A month after its preparation the lead complex solution begins to show phenomena of ageing, which result in thinner films of a poor quality.

IV. **Conclusions** From our experiments we may conclude that the chemical deposition procedure of PbSe films is a complex process, which may be controlled only if all reaction parameters are strictly kept under control

Sodium selenosulfate is prepared more easier than selenourea which asks for organic sinthesis and the use of hydrogen selenide, a highly toxic substance. Sodium selenosulfate has a greater stability in aqueous solutions than selenourea, so longer reaction times can be achieved more easily.

The properties of the films grown by this method by using sodium selenosulfat are. the qualities of the surface, its thickness, photoconduction, etc. are as good as those obtained on deposited films using selenourea.

The most important factors conditioning the quality of the films are: pH of the deposition solution, the concentration of the reactants, bath temperature, and deposition time.

REFERENCES

1 D. G. Coates, J. Electrochem Soc, **110**, 174—5 (1963)
2 R B Schoolar, J R Lowney, J. Vac Sci Technol, **8 (1)**, 224—7 (1971)
3. C J Milner, B. N Watts, Nature, **163**, 322 (1949)

4 B N Mc Lean, U S 2, **997,** 409 Aug 22, (1961)
5 R. A Zıngaro, D O Skovlın, J Electrochem. Soc, **111 (1),** 42—**7** (1964)
6 G. M Fofanov, G A Kıtaev, Zh Neorg Khım, **14 (3),** 616—20 (1969)
7. G S Klebanov, N A. Ostapkevıch, Zh Prıkl Khım, **33,** 1957—61 (1960)
8. N. I Glıstenko, A A Eremına, Zh. Neorg Khım, **5 (5),** 1003—**5** (1960)
9 N I Glıstenko, I. N Shramchenko, A. N Kosılova, Zh. Prıkl. Khım, **45 (6),** 1356—7 (1972)
10. R. M Cândea, D Dădârlat, P Fıtorı, R Turcu, E Indrea, Al. Darabont, L P Bıró, I. Bratu, N Aldea, Studıı şı Cercetărı de Fızică, **38 (4),** 410—20 (1986)
11 R. M. Cândea, R. Turcu, P. Mărgınean D. Dădârlat. Phys. Status Sol., (a), **96,** 337—43 (1986)

STUDIA UNIV BABEŞ—BOLYAI, PHYSICA, XXXI, 2, 1986

THE FERROMAGNETIC LINE IN POROUS RARE EARTH GARNETS

D. IANCU* and D. STĂNILĂ*

Received November 14, 1986

ABSTRACT — The paper shows how effective ferromagnetic linewidth, in polycrystalline Tb, Y, Yb garnets is broadened by the presence of pores. This fact is important for the use of these garnets when are applied to microwaves filters in a larger or smaller band of frequency in function of necessities.

Introduction In polycrystalline garnets consisting of randomly oriented crystallites, the angle between the applied field and the crystal axis, varies through all values. The effect of this is broadening the resonance absorbtion line. Similarly, the demagnetising effect, voids, stresses, which can be produced during the sintering process, or inhomogeneous regions also broadens the resonance [1]. In this paper we take into account only the dependence between the effective resonance linewidth and the average diameter of pores, [2] in polycrystalline rare earths. The porosity of samples may be controlled by pressing the material before the sintering process.

Preparation of samples. The powder of the constituent materials, rare earth oxide R_2O_3 (R may be Tb, Y or Yb) and hematite Fe_2O_3 with three nine purity, were mixed in the proper ratio with an organic liant, in water, for six houres. Then the mixture was warmed up until complet elimination of water. Then the obtained mixture was pressed at various degrees of pressing varying between 20 and 100 Kgf/cm^2.

After having pressed them, the samples were sinterised in an oxidant atmosphere, according with the following thermal diagrame (Fig. 1). In this way were obtained cylindrical samples of the two milimeter diameter and two milimeter highness with different porosity.

Results. By the analysis of ferromagnetic resonance in a TE_{011} mode cylindrical microwave (X-band) resonant cavity of rare earth samples, the dependence of resonance linewidth versus volum of pores is presented in Fig. 2. For small porositys, from the figure, an almost linear dependence may be seen. Here the resonance line broadening is proportional to the product of volume fraction of effective porosity, and $4\pi M_s$, the saturation magnetization [3]. For larger porositys, the low becomes almost nonlinear. Through

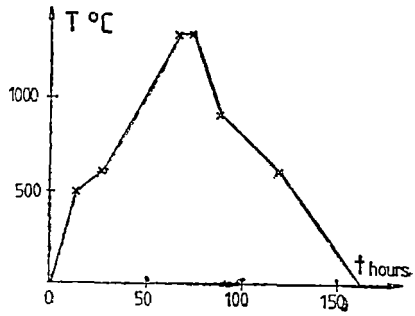

Fig. 1. Heating diagram.

* *University of Cluj-Napoca, Department of Physics, 3400 Cluj-Napoca, Romania*

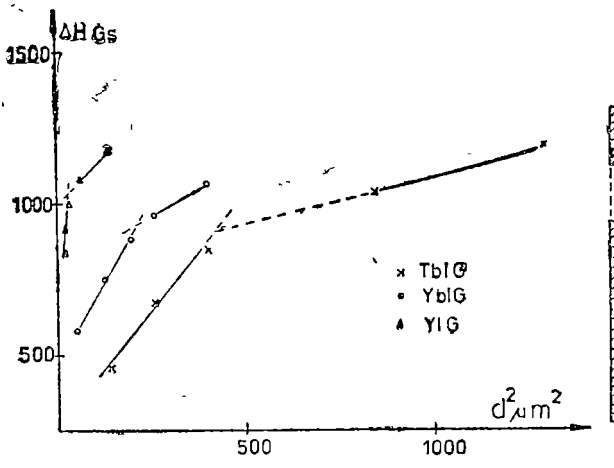

Fig 2 Linewidth dependence as a function of the porosity for TbIG, YIG and YbIG

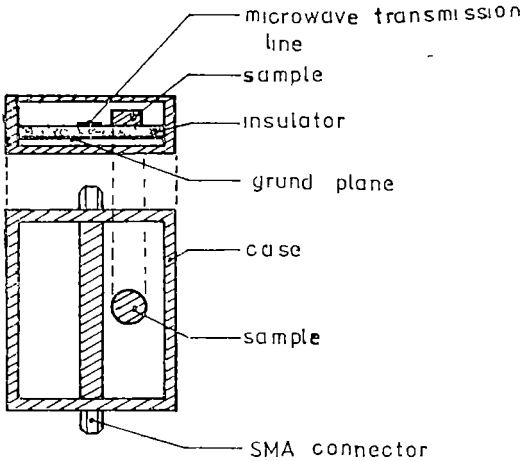

Fig 3 Schematic of the microstrip structure used in measuring of the absorbed power as a function of the applied d c. magnetic field.

incorporation of the samples into the (X-band) microstrip line (Fig. 3) absorbed microwave power, in function of d.c. magnetic field, applied parallel to the rare earth garnet samples axis, appear on Fig. 4, Fig 5 and Fig. 6.

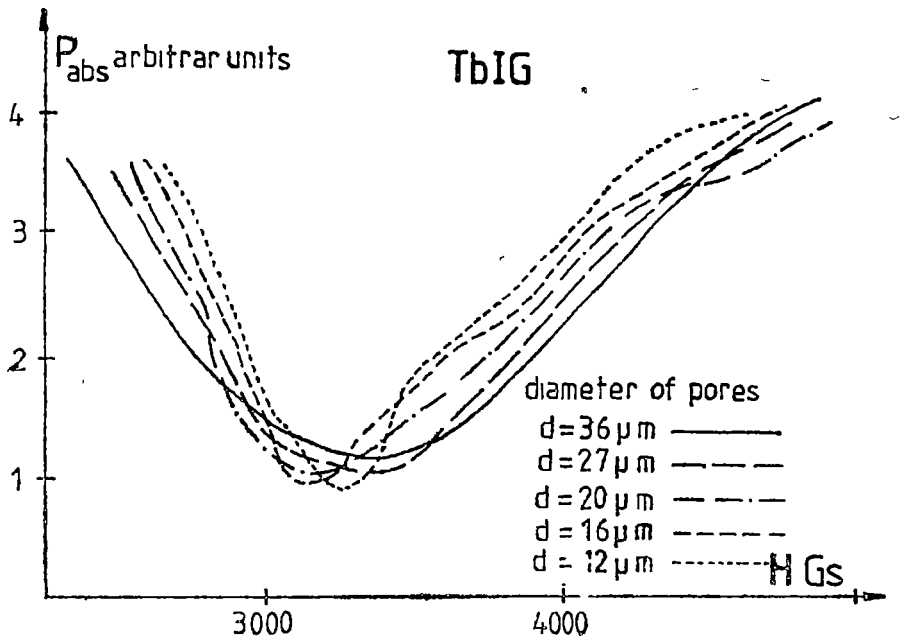

Fig 4. Absorbed power dependence as a function of the applied d c magnetic field for the TbIG.

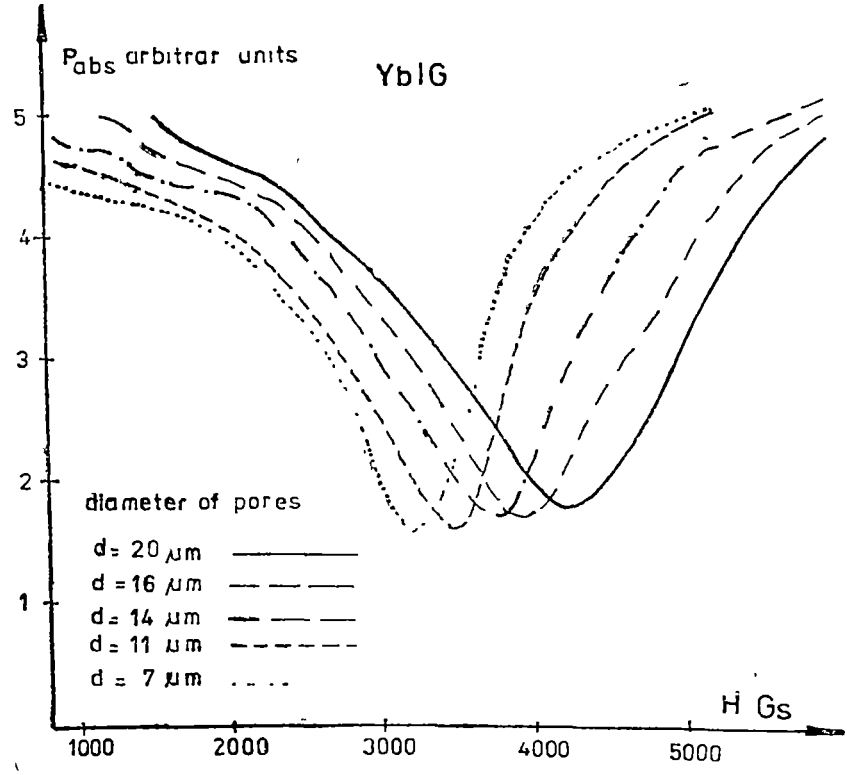

Fig 5 Absorbed power dependence as a function of the applied d c magnetic field for the YbIG.

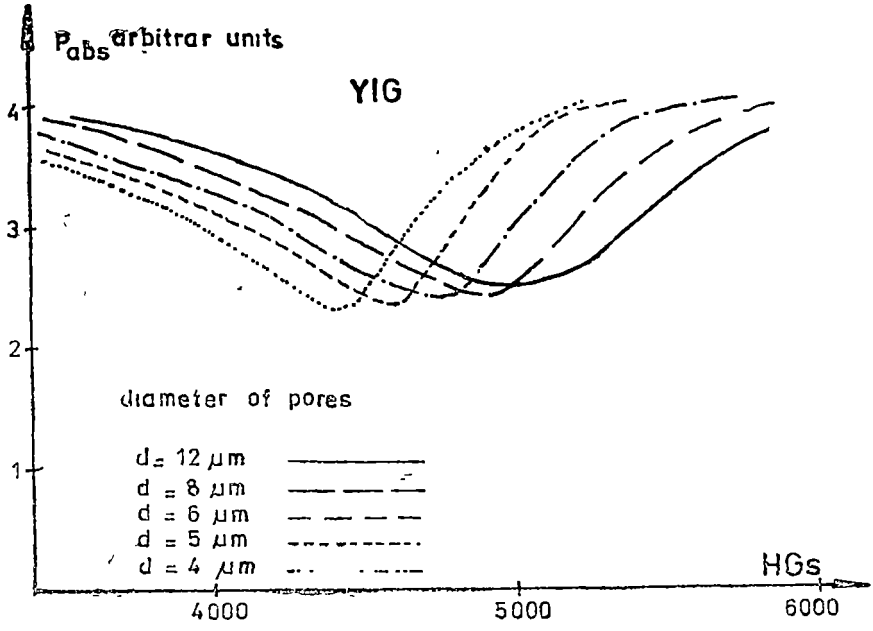

Fig 6 Absorbed power dependence as a function of the applied d c. magnetic field for the YIG.

REFERENCES

1. Q H F Vrehen, J. Appl. Phys , **40** 1849 (1969)
2 E. Schloemann, in Proc. Conf on Mag and Mag. Mat IEEE Spec Publ. T—91 (1957) p. 600
3. F. Dionne, Mat Res. Bull., **5** 939 (1970)

STUDIA UNIV BABEŞ—BOLYAI, PHYSICA, XXXI, 2, 1986

A GENERATOR FOR LINEAR RECORDINGS OF SPECTRA

V. IONCU*, Gh. CRISTEA* and E. TĂTARU*

Received November 14, 1986

ABSTRACT. — We have designed and set up a generator for linear sweeping of the detecting-oscilators frequency used in the equipment for differential recording of Quadrupolar Nuclear Resonance (QNR) signals The generator can be succesfully used for sweeping of the magnetic field and the frequency in the equipment with linear display of high resolution Nuclear Magnetic Resonance (NMR) spectra At the same time the generator has been proved as a first hand accessory in the equipment for the study of the metal-dielectric-semiconductor (MDS) structures

General account. As it is known [1, 3, 7], usually, the obtaining of a linear varable voltage (LVV) is the result of charging or discharging of an electric condensor across a dipol The charging or discharging dipol is a circuit which must ensure a charging or discharging current for the condensers The principle scheme, most often used, for generation of LVV is presented in Fig. 1, and is set up on an integrator of the analogic signal.

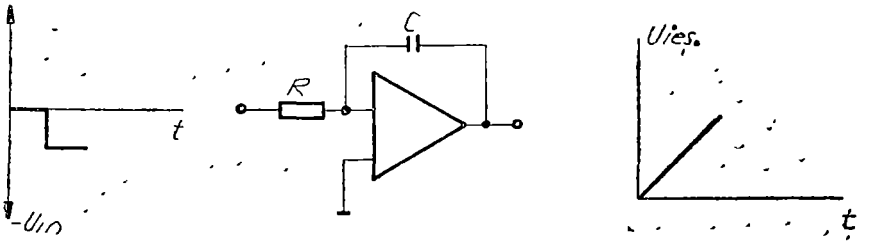

Fig 1

If the imput signal is a direct voltage or has a rectangular form, the output voltage is given by the integral of the imput signal

$$U_{out} = \frac{1}{C}\int i dt \qquad (1)$$

From (1) results that a constant charging current is maintained during the whole active course.

Combinations of integrating and comparating circuits are used for the generation of linear variable voltage [4, 5, 6] (Fig 2). The combinations can be performed with one or

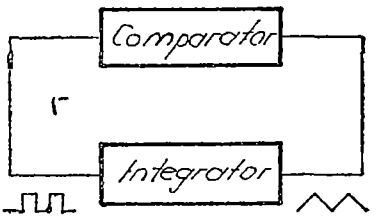

Fig 2

* *University of Cluj-Napoca, Department of Physics, 3400 Cluj-Napoca, Romania*

more operational amplifiers. The comand of amplitude, period and shape of the signal at the output of the integrator can be achived in several ways:

— The rectangular voltage supplied usually by the comparator, comanded by the level of the output voltage, is applied at the imput of the operational amplifier. It depends on the elements of the circuit whether the LVV is symmetric or asymmetric with respect to zero

— The imput of the integrator is fed with constant voltage and the return to the initial state is ensured by means of a comand device which acts like a rely, or an electronic commutator which shorten, at a particular moment, the condenser C discharging it in a very short time With such a comand of the integrator a positive or negative LVV is ontained. (The discharge time is neglijable as compared with the time of the useful course)

The time of the active course of usual LVV generators may vary within a rather wide range, from $0{,}5 \cdot 10^{-7}$ s to 1800 s [2, 7]. The upper limit of this period of time (which is of interest for us) is determined by maximum values of the capacities of the condensers with convenient size and weight, by the maximum values of the resistens of the charging resistors (including the losses) and by the minimum currents at which the active elements are still satisfactory functioning [8, 9]. The integration precision is determined mainly by the losses in the condensers which are small in condensers with synthetic dielectrics (polystyrole, polycarbonates, polyetilenterephtalate) which have $\rho_{izol} > 10^{12}\ \Omega.m$.

The main problems we had to solve in order to set up a LVV generator, having a long enough active sweeping time and a degree of nonlinearity as low as possible, can be summarized as folows

a) to build up a constant current generator with high imput impedance and high stability of the suplied current,

b) to build up an electronic commutator for the condenser discharge which shunts the integrating condenser as litle as possible during of the the active course;

c) to devise an integrating condenser of high capacity, with small loss current, at convenient size and weight,

d) to find condensers having good time stability as well as against the temperature variations,

e) to ensure a long time stability for the functional parameters of the apparatus and against temperature variations;

f) to reduce the external influences on the functional parameters of the apparatus.

Description of the generatior. The principle scheme of the LVV generator is presented in Fig. 3. It consists of the following functional blocks:

1) the capacity multiplier built on the operational amplifier AO_1 working as an integrator; 2) the noninveisor follower stage AO_2, 3) the AO_3 comparator, 4) the matching circuit in TTL logic (D_1, D_2, H_1); 5) the electronic commutator T_1, popeily comanded by the group consisting of the tact generator (H_3, H_4), the bistabile I_1 and the commutator-comparator AO_4, 6) the constant current generator (AO_5, T_2), fed with a double stabilized voltage (I_2

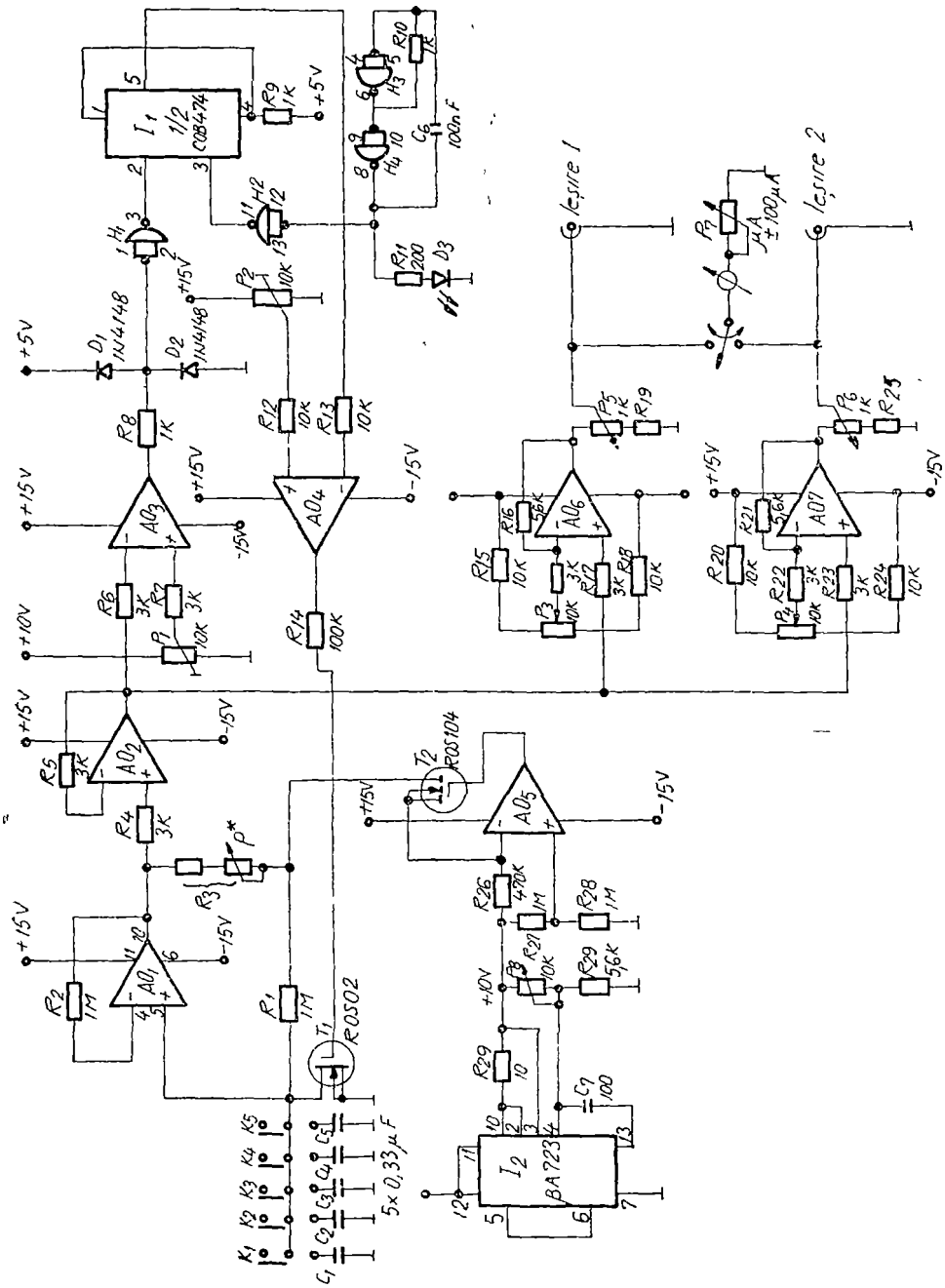
I1 1/2 CD8474
H1
H2
H3
H4
D1 1N4148
D2 1N4148
D3
R1 1M
R2 1M
R3 P*
R4 3K
R5 3K
R6 3K
R7 3K
R8 1K
R9 1K
R10 1K
R11 200
R12 10K
R13 10K
R14 100K
P1 1M
P2 10K
P3 1K
P4 10K
P5 1K
P6 1K
R15 10K
R16 56K
R17 3K
R18 10K
R19
R20 10K
R21 56K
R22 3K
R23 3K
R24 10K
R25
R26 470K
R27 10K
R28 1M
R29 10
R29 56K
C1
C2
C3
C4
C5
5x 0,33 μF
C6 100nF
C7 100
T1 BD502
T2 BD5104
I2 BA7234
AO1
AO2
AO3
AO4
AO5
AO6
AO7
+15V
-15V
+10V
+5V
Ieşire 1
Ieşire 2
μA ±100μA
K1
K2
K3
K4
K5

Fig 3

is the second stabilizer); 7) the output amplifiers (AO_6, AO_7), which also regulate the range of the output voltage.

The scheme of the stabilized voltage supply at $\pm$ 15 V and respectively at +5V is given in Fig. 4.

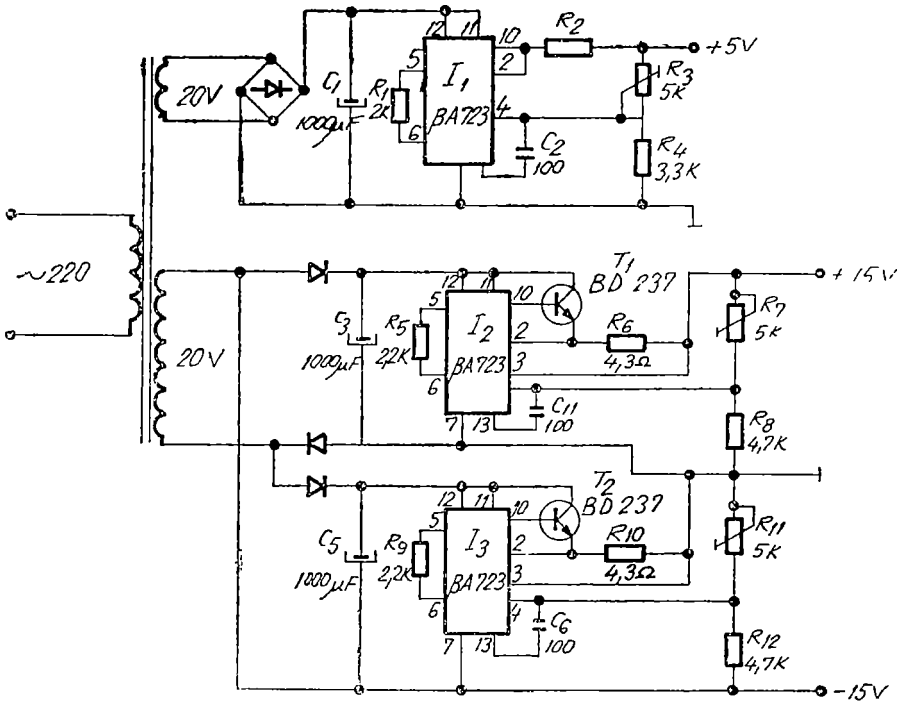

Fig 4

At the basis of the generator functioning lies the charging of the group of $C_1 - C_5$ condensers by the current supplied by the constant current generator and the obtaining of variable voltage of very low degree of nonlinearity at the output of the operational amplifier O_1A To get rid of the influences which the output load might have on the integrator characteristics its output voltage is fed to the comparator AO_3 and to the output amplifiers AO_6 and AO_7, by means of the noninversor stage follower OA_2 At the moment when the voltage reaches the threshold level, established with the trimer P_1, the comparator swiches To avoid the ,,anchorage'' of the electronic commutator in an undefined regim we have introduce the state determining group, consisting of I_1, H_3, H_4 and OA_4, which alows to take over the state from the data imput of the bistabile I_1 and transfering it to the electronic commutator T_1 in the corresponding logic (closed or open) At the predetermined time the commutator T_1 alows the rapid discharge of the condenser group $C_1 \div C_5$ and taking again the work cycle

The capacity multiplier. Since the electrolytic condensers of high capacity do not satisfy the requirments in items c) ÷ e) above, we made use of the following trick. In the $C_1 \div C_5$ group we have used polyester condensers whose individual capacity does not exceed 2 μF, but together with the operational amplifier OA_1 forms a capacity multiplier. When the amplification of OA_1 is much biger then the unit (this requirement is easily fulfield by any operational amplifier) the imput impedance of this scheme is

$$Z_i = \frac{U_i}{I_i} = \frac{R_1 R_3}{R_1 + R_3} + \frac{1}{j\omega C_1} \cdot \frac{R_3}{R_1 + R_3} \tag{2}$$

where we supposed that only the C_1 condenser is introduced in circuit If one choses $R_1 \gg R_3$ we have

$$Z_i \cong R_3 + \frac{1}{j\omega C_1 \frac{R_1}{R_3}} \tag{3}$$

One can see from (3) that the imput impedance of the circuit consists of the R_3 resistor, of very small value connected in serie with equivalent condenser

$$C_e = \frac{R_1}{R_3} C_1 \tag{4}$$

of vary large capacity, whose reactance is $X_{Ce} = 1/C_e\omega$. The multiplier factor is, evidently, the ratio R_1/R_3 which can be made quite big

Naturally, the amplified equivalent capacity C manifests itself only in dynamic regim In stationary regim the charge stored by the condenser remains equal to C_1U_1

In order to reduce the effect of the lagging current of the operational amplifier the value of the resistor R_2 has been chosen equal to that of R_1. The value of the multiplier factor R_1/R_2 may be modified according to the necesities, by means of the P^* potentiometer The value of the multiplied charge is chosen by means of commutators $K_1 \div K_5$.

Constant current generator. As for the chosen working variant a single polarity of the output current is needed, we have built the constant current (c c) generator on the operational amplifier OA_5 and the MOS transistor T_2

The imput impedance of the c c. dipol is of the order of hundreds of $M\Omega$, i.e in agreement with the requirement stated above, in item a). In fact, the stability of the c c. generator depends only on the refference voltage supplied at the imput of the operational amplifier OA_5, since $I = E_{reff}/R_{37}$ For this reason we have resort to: 1) a double stabilisation by means of the I_2 stabiliser, 2) mentaining the gait-sourse voltage at a value near to zero, 3) usage of some metal thin film risistors.

The electronic commutator. The rol of the electronic commutator T_1 is played again by a MOS transistor. During the time in which the gait voltage is negative (—10V), and it coincides with the logic level L at the output Q of the bistabile I_1, the C_e condenser will be charging in a c.c. regime. The very large drainesourse resistens (hundred of $M\Omega$) of the MOS transistor in blocked regim is in paralel with the condenser, which strongly attenuates the

sunting effect, as well as the alteration of the charging characteristic of the condenser When the voltage across the MOS transistor jumps from the negative (−10V) to the positive (+10V) value, a value which is equal with the level of the logic H at the Q output of the bistabile, the transistor opens (the saturation is reached) and the condensor is rapidly discharging through it (the drain-sourse resistence has low value) The charging time of the condenser is much longer then the discharging time

As we have mentioned above, the TTL logic adaptor, the formation gate H_1, the bistabile I_1 and the tact generator H_3, H_4, have been introduced in order to rigurously determinate the states of the electronic commutator, in agreement with the states of the AO_3 comparator as well as for an automatic starting of a new integrating cycle

The tipping level of the comparator is regulated by means of the trimmer potentiometer P_1 and was set to supply a maximum voltage of +5V at the OA_2 output

The output amplifiers OA_6 and OA_7 alow the selection of the variation range of the output voltage, of maximum amplitude (10V), between −10V and +10V The choice of the working domain is done by P_3 and P_4 potentiometers, while the level of the output voltage is selected by P_5 and P_6 potentiometers

The amplitude of the linear variable voltage suplied by the generator is adjustable whithin the range of $\pm$10V and sweeped during a period of time between $0\,1 - 4 \cdot 10^3$ s The generator also allows the control of the output voltage amplitude, independent of its sweeping speed The nonlinearity of the output voltage is less then 0 15% for all amplitude and duration ranges

REFERENCES

1 P J Vabre, *Electronique de impulsions*, Tom 3, *Les generateurs de impulsions*, Paris, 1970
2 Gh Mitrofan, *Generatoare de impulsuri şi de tensiune liniar variabilă*, Ed „Tehnică", Bucureşti, 1969
3 R L Moris, J R. Miller, *Proiectarea cu circuite integrate TTL*, Ed „Tehnică", Bucureşti, 1974
4 J Graeme, *Application of operational amplifiers Third-Generation Techniques*, New-York, 1972
5 D Rana, B K Dispak, K. Prodip, Voltage-controlled oscilator provides symetrical triangular and square waves forms, Electronic Design 24, 1976
6 W J Woodword, Inexpensive triggered-sweep generator up-dates recurring-sweep scopes. Electronic Design 23, 1976
7 Gh Mitrofan, *Generatoare de impulsuri şi de tensiune liniar variabilă*, Ed „Tehnică", Bucureşti, 1979
8. A Zagrubskii, V A Lovitzius, V V Petrov, Priborî i Tehnica Experimenta 1, **128,** 1980
9 B F Alexeev, A I Manrikin, Priborî i Tehnica Experimenta 5, **281,** 1976

STUDIA UNIV BABEŞ—BOLYAI, PHYSICA, XXXI, 2, 1986

BLOCH EQUATIONS IN MAGNETIC RESONANCE SPIN IMAGING

Al. NICULA* and S. NICULA*

Received November 18, 1986

ABSTRACT. — The paper presents the Bloch equations as being applied in magnetic resonance spin imaging technique Both, constant field gradient and dipolar field where used. The Bloch equations were resolved for the stationary and unstationary states A special attention is accorded to the dependence on the dipolar field or on the field gradient of the absorbted power, which also depends on the spin moment concentration

Introduction. In a previous paper we contributed to a study of EPR spin imaging using, as aditional magnetic field, a dipolar field produced by a permanent magnet or by a coil, having a proper magnetic moment $\vec{m}$ In the same paper we used also, a liniar field gradient for studying spatial EPR of DPPH and a glass containing molibden paramagnetic ion [1].

In both cases the Hamiltonian for an isolated spin in a magnetic field, including dipolar or gradient, is

$$H = \hbar\omega_0 S_z + \hbar\vec{S}\cdot\tilde{F}\cdot\vec{r} \tag{1}$$

where $\tilde{F}$ is a tensor comprising nine components and which for field gradient is written as

$$\tilde{F} = \begin{Bmatrix} \frac{\partial B_x}{\partial x} & \frac{\partial B_x}{\partial y} & \frac{\partial B_x}{\partial z} \\ \frac{\partial B_y}{\partial x} & \frac{\partial B_y}{\partial y} & \frac{\partial B_y}{\partial z} \\ \frac{\partial B_z}{\partial x} & \frac{\partial B_z}{\partial y} & \frac{\partial B_z}{\partial z} \end{Bmatrix} \tag{2}$$

The product $\tilde{F}\cdot\vec{r}$ can be transformed into a vector field $\Delta\vec{B}$ with three components along the principal axis. When the main static field $\vec{B} = \vec{k}B_0$ is added, the components $\Delta\vec{B}_x i$ and $\Delta\vec{B}_y j$ can be discarded provided that $B_0 \gg |\Delta B|$. Upon examination of the relation (2) we see that discarding these components is equivalent to retaining the battom row only of $\tilde{F}$ in Eq. (2), and the product $\vec{S}\cdot\tilde{F}$ becomes $S_z\vec{F}$, where the vector $\vec{F}$ has the components $F_x = \partial B_z/\partial x$, $F_y = \partial B_z/\partial y$, $F_z = \partial B_z/\partial z$. In the case of dipolar field the tensor

* *University of Cluj-Napoca, Department of Physics, 3400 Cluj-Napoca, Romania*

F from the second term of Eq. (1) becomes a vector field B_d which is connected with the magnetic moment $\vec{m}$ by the relation, [2]

$$\vec{B}_d = \frac{\mu_0}{4\pi}\left[-\frac{\vec{m}}{r^3} + 3\frac{(\vec{m}\ \vec{r})\cdot\vec{r}}{r^5}\right] \tag{3}$$

where $\vec{r}$ determines the position of an isolated spin If the magnetic moment $\vec{m}$ is parallel with the main static field $\vec{k}B_0$, the relation of Eq (3) becomes

$$B_d^z = \frac{\mu_0}{4\pi}\frac{m}{r^3}(3\cos^2\theta - 1)$$

and

$$B_d^1 = \frac{\mu_0}{4\pi}\frac{3m}{r^3}\cos\theta\sin\theta \tag{4}$$

in spatial transitions being important the first relation of Eq (4), considering again that $B_0 \gg B_d$

Bloch Equations of the Spin Sistem. We shael restrict our discussion of imaging techniques to noninteracting, or weakly interacting spin system In this case the spin magnetization behaves classically and is described by Bloch equations [3] in which relaxation processes are added

We consider the vector form of the Bloch equations [4] The total magnetization vector in the laboratory frame is

$$\vec{M} = \gamma\hbar\sum_i \vec{S}_i \tag{5}$$

The Bloch equations in the laboratory reference frome becomes

$$\begin{aligned}
\frac{dM_x}{dt} &= \gamma(B_z M_y - B_y M_z) - \frac{M_x}{T_2}\\
\frac{dM_y}{dt} &= \gamma(B_x M_z - B_z M_x) - \frac{M_y}{T_2}\\
\frac{dM_z}{dt} &= \gamma(B_y M_x - B_x M_y) - \frac{M_z - M_0}{T_1}
\end{aligned} \tag{6}$$

where B_x, B_y and B_z are the components of vector $\vec{B}$ which has the form

$$\vec{B} = \vec{k}B_0' + \vec{B}_1(t) \tag{7}$$

with Zeeman term field as

$$B_0' = B_0 + \vec{F}\cdot\vec{r}$$

and M_0 being the thermal equilibrium magnetization The terms T_1 and T_2 are the spin-lattice and spin-spin relaxation times respectively The radio

frequency field $\vec{B}_1(t)$ rotates with angular frwquency ω close to the spin Larmor frequency and has the from

$$\vec{B}_1(t) = \vec{\imath} B_1 \cos \omega t - \vec{\jmath} B_1 \sin \omega t \tag{8}$$

The expanded Eqs. (6) may be written compactly in the matrix form as

$$\frac{d\tilde{M}}{dt} = \tilde{L}\tilde{M} + \left(\frac{M_0}{T_1}\right) \tag{9}$$

where $\tilde{M}$ is naw a calumn matrix and the laboratory frame evolution matrix $\tilde{L} = \tilde{N} + \tilde{D}$ is gibven by

$$\tilde{L} = \begin{bmatrix} -\frac{1}{T_2} & \gamma B_0' & \gamma B_1 \sin \omega t \\ -\gamma B_0' & -\frac{1}{T_2} & \gamma_1 B \cos \omega t \\ -\gamma B_1 \sin \omega t & -\gamma B_1 \cos \omega t & -\frac{1}{T_1} \end{bmatrix} \tag{10}$$

where $\tilde{N}$ and $\tilde{D}$ are the nondiagonal and diagonal parts of the matrix $\tilde{L}$ respectively.

We define u to be the component of (M_x, M_y) which is in phase with the B_1 field and v to be perpendicular component wich is 90° aut of phase. In matrix form the transformation equation can be expressed as

$$\begin{bmatrix} M_x \\ M_y \end{bmatrix} = U \begin{bmatrix} u \\ v \end{bmatrix} \tag{11}$$

where

$$U = \begin{bmatrix} \cos \omega t & -\sin \omega t \\ -\sin \omega t & -\cos \omega t \end{bmatrix} \tag{12}$$

and by inversion of the matrix, we obtain

$$\begin{bmatrix} u \\ v \end{bmatrix} = U^{-1} \begin{bmatrix} M_x \\ M_y \end{bmatrix} \tag{13}$$

Applying this linear transformation U^{-1} to a new reference frame rotating about the z axis at angular frequency ω the Eq (9) becomes

$$\frac{d}{dt} \begin{bmatrix} u \\ v \\ M_z \end{bmatrix} = Q \begin{bmatrix} u \\ v \\ M_z \end{bmatrix} + \frac{M_0}{T_1} \tag{14}$$

where Q has the form

$$Q = \begin{bmatrix} -\frac{1}{T_2} & -\Delta\omega & 0 \\ \Delta\omega & -\frac{1}{T_2} & -\omega_1 \\ 0 & \omega_1 & -\frac{1}{T_1} \end{bmatrix} \tag{15}$$

The unknown simbols in this matrix are $\Delta\omega_0' = \omega_0' - \omega$, $\omega_1 = \gamma B_1$ and $\omega_0' = \gamma B_0'$

The steady-state conditions imply that u and v as well as M_z are constant. In this case we simply solve the equation

$$Q \begin{bmatrix} u \\ v \\ M_z \end{bmatrix} + \begin{pmatrix} M_0 \\ T_1 \end{pmatrix} = 0 \tag{16}$$

If we use relation (13) and the third Eq of (6), and making same simple algebric manipulations, [5] the steady-state solutions of Bloch equations in the laboratory frame are

$$\begin{aligned} M_x &= \frac{1}{2} M_0 \gamma T_2 \frac{T_2(\omega_0' - \omega)\, 2B_1 \cos\omega t + 2B_1 \sin\omega t}{L(\omega_0' - \omega)} \\ M_y &= \frac{1}{2} M_0 \gamma T_2 \frac{2B_1 \cos\omega t - T_2(\omega_0' - \omega)\, 2B_1 \sin\omega t}{L(\omega_0' - \omega)} \\ M_z &= M_0 \frac{1 + T_2^2(\omega_0' - \omega)^2}{L(\omega_0' - \omega)} \end{aligned} \tag{17}$$

where $L(\omega_0' - \omega) = 1 - \gamma^2 B_1^2 T_1 T_2 + T_2^2(\omega_0' - \omega)^2$. We see that stady-state solution depends of B_0' which contains a linear gradient field ΔB or a dipolar field B_d

Energy Absorationin in Spatial Magnetic Resorance. Let us analyse power absorbed by sample form the B_1 field. The mean rate of energy absorbtion, per unit volume of sample, which containes N spins, is given by

$$A = \left\langle B_x \frac{dM_x}{dt} \right\rangle = \frac{\gamma\omega B_1 M_0 T_2}{1 + T_2^2(\omega_0' - \omega)^2 + \gamma^2 B_1^2 T_1 T_2} \tag{18}$$

If $\omega_0' = \omega_0$, namely $\gamma B_0'$ do not contains field gradient or dipolar field being equal with B_0, A goes through a maximum as would be expected The power absorbtion can be expressed in terms of χ'' susceptibility and it is find that

$$A = 2\omega B_1^2 \chi'' \tag{19}$$

where

$$\chi'' = \frac{1}{2} \chi_0 \omega_0 \frac{T_2}{1 + \gamma^2 B_1^2 T_1 T_2 + T_2^2(\omega_0 - \omega)^2} \tag{20}$$

χ_0 is the equilibrium static susceptibility defined for the spin 1/2 case by

$$\chi_0 = \frac{M_0}{B_0} = \frac{N\mu^2}{kT}$$

We devive our expression for power absorbed containing the line shape function $g(\omega)$, [6]. The population change caused by induced transition between the $-1/2$ and $+1/2$ states is

$$P(n_+ - n_-) = \frac{1}{4}\gamma^2 B_1^2 g(\omega)\,(n_+ - n_-) =$$

$$= \frac{1}{4}\gamma^2 B_1^2 g(\omega)\left[\frac{N}{2}\left(1 + \frac{\mu_0 B_0}{kT}\right) - \frac{N}{2}\left(1 - \frac{\mu B_0}{kT}\right) = \frac{1}{4}\gamma^2 B_1^2 g(\omega)\frac{N\mu B_0}{kT}\right] \tag{21}$$

Since each of the net upward transition requires the absorbtion of a quantum of energy $h\nu$ we write

$$A = \frac{1}{4}\gamma^2 B_1^2 g(\omega)\frac{N\mu B_0}{kT}\,h\nu \tag{22}$$

We see from this equation that energy absorbed depends of N, the number of spins per unit volume. If now B_0 is changed by adding a field gradient or a dipolar field we can map, using a computing system, the density of spins from sample. In this case A becomes a function of ω_0', namely of B_0' and in the same time it is a function of N.

If u and v as well as M_z depend on time we have to aslve Eq. (14) which is a differential equation of Bernoullin type Noting with $P(t)$ the colomn matrix of Eq. (14), it is helpful in considering the solution of Bloch equations in this case, to split Q into two parts, i.e., $Q = A + T$, where the first term involves no relaxation terms and from Eq. (15) is given by

$$A = \begin{bmatrix} 0 & -\Delta\omega & 0 \\ \Delta\omega & 0 & -\omega_1 \\ 0 & \omega_1 & 0 \end{bmatrix} \tag{23}$$

and the diagonal relaxation term is simply

$$T = \begin{bmatrix} -\frac{1}{T_2} & 0 & 0 \\ 0 & -\frac{1}{T_2} & 0 \\ 0 & 0 & -\frac{1}{T_1} \end{bmatrix} \tag{24}$$

with these remarks, the Eq. (14) becomes

$$\frac{dP(t)}{dt} = QP(t) + \frac{M_0}{T_1} \tag{25}$$

and the solution of this equation is

$$P(t) = e^{At}E(t)\chi(t)P(0) + M_0(1 - E_1) \tag{26}$$

where $E(t)$ is a relaxatıon type matrix gıven by

$$E(t) = e^{Tt} = \begin{bmatrix} E_2 & 0 & 0 \\ 0 & E_2 & 0 \\ 0 & 0 & E_1 \end{bmatrix} \tag{27}$$

n which $E_1 = e^{-t/T_1}$, $E_2 = e^{-t/T_2}$ and $\chi(t) = e^{-Tt}\, e^{-At}\, e^{Qt}$ since A and T do [1]not comute in general [7]. The term $P(0)$ is the intral value of $P(t)$ at $t = 0$.

REFERENCES

1 Al Nıcula, S Nıcula, L Giurgıu, I Ursu, *EPR spın ımagıng usıng dıpolar fıelds*, Studıa—Physıca, **XXXI** (1), 1986, p 3
2. Al. Nıcula, *Electrıcıtate şı magnetısm*, EDP Bucureştı, 1973
3. I. Ursu, *La Resonance Paramagnetıque Electronıque*, Dunod—Parıs (1960)
4. R Freeman and N. D W. Hıll, J. Mag Reson. *4*, 366 (1971)
5. H G Hecht, *Magnetıc Resonance Spectroscopy*, John, Wıley, N Y 1967
6. Al. Nıcula, *Rezonanţă Magnetıcă*, EDP — Bucureştı, 1975
7. P. Masfıeld and P. G Morrıs, *NMR Imagıng ın Bıomedıcıne*, Academıc Press, N.Y. (1982)

STUDIA UNIV BABEŞ—BOLYAI, PHYSICA, XXXI, 2, 1986

TRITIUM ACTIVITIES IN CLUJ-NAPOCA RAINFALL

I. CHEREJI*

Received November 27, 1986

ABSTRACT. — A brief account is given on the method of analyzing tritium abundences from the samples collected in Cluj-Napoca between 1978—1984 The measurement results point to seasonal variations of tritium concentrations, with maxima in summer, as well as to a recurrent trend towards the level extant before the first thermonucleary weapon experiences

Results of the measurements for 1978—84 period are presented.

A proportional gas counting method is used for the measurement of low-level tritium activities Firstly, the water samples are distilled to dryness. Then an isotopic enrichment procedure by electrolysis is apllied. The electrolytic cells (cathode of mild steel and anode of stainless steel) containing 250 ml of 1% NaOH solution are operated at the same current intensity and temperature After an adequate chemical treatment [1] a protium-tritium separation factor β of 11—12 is obtained. The separation factor is calculated from the relation $\lg \beta = 1{,}4 \lg \alpha$, where the protium-deuterium separation factor α is measured by mass-spectrometry When the electrolysis is over the samples are neutralized with $PbCl_2$ [2] and redistilled.

Completely labelled ethane is used as internal gas sample for the proportional counter. The ethane preparation consists of three steps [3] :

(1) preparation of acetylene

$$2H_2O + CaC_2 \rightarrow C_2H_2 + Ca(OH)_2$$

(2) water hydrogen conversion at 600°C

$$H_2O + Mg \rightarrow H_2 + MgO$$

(3) ethane synthesis in the presence of Pd catalyst

$$C_2H_2 + 2H_2 \rightarrow C_2H_6.$$

In this way all six hydrogen atoms of the filling gas molecule arise from the active sample. The counting sensitivity of 0 5 1 counter filled at 1 atm is about 1 cpm/TU (1 TU = 10^{-18} T/H). With a multifilar guard counter [4] operating in anticoincidence and by shielding with 2.5 cm Hg and 15 cm Pb the background of the sample counter is about 2 cpm.

The block diagram of the electronic equipment is shown in Fig. 1.

The count-rate from the tritium channel, total main counter and guard counter are printed every 20 minutes. In a total counting time of 24 hours

* *Institute of Isotopic and Molecular Technology, 3400 Cluj-Napoca, Romania*

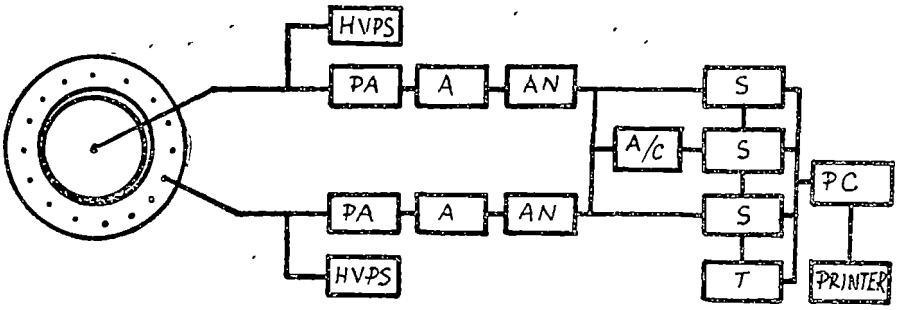

Fig 1

the accuracy obtained is about 18% for a sample of 25 TU and up to 8% for a sample of 50 TU.

The results of the measurements are represented in Fig 2

In the first two years (1978—79) the tritium activities were monthly measured and then only once for each quarter of the year. From these data we may conclude the following

Firstly, it is easy to see the well-known seasonal variation of the activities, the summer values corresponding to a greater transport rate of the rainfalls.

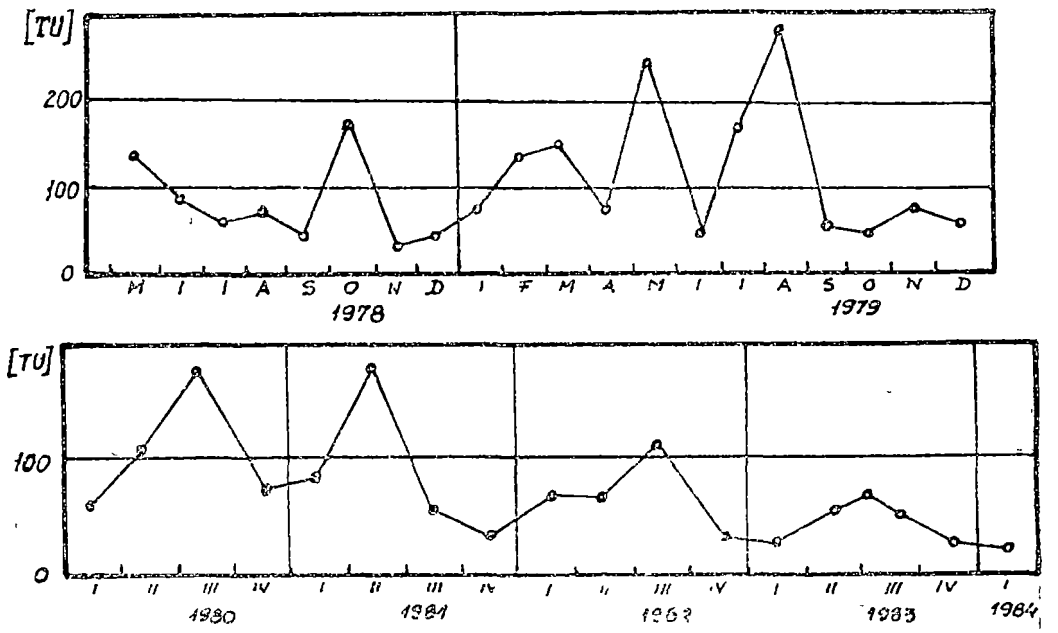

Fig. 2

Secondly, the most important fact is that the mean values up to the beginning of 1984 are tending to the natural concentrations measured before H-bomb explosions in atmosphere

REFERENCES

1 IAEA Laboratory Report, May 1967
2 D J Groeneveld, Thesis, Univ Groningen, 1977
3 I Cherejı, J Radioanal Chem , **46**, 67 (1978)
4 I Cherejı, Proc Nat Conf Phys., Sibiu, 636 (1984)

STUDIA UNIV BABEŞ—BOLYAI, PHYSICA, XXXI, 2, 1986

A MICROPROCESSOR SYSTEM IN DIDACTIC PURPOSE

G. VARGA*, G. D. POPESCU*

ABSTRACT. — Getting familiarized with the functioning and world-wide use of microprocessors is often ressented with necessity The paper presents a microsystem which can be used in educational purpose As units to be used together with standard chips of a μP system some easy to build and interpret circuits are described

Within the last years the microprocessors have continued to be used in the most varied fields of activity. As it has become a basic element in physics too, in the automatization of data processing and in the work principle of measuring and control apparatus, the microprocessor must be known by its future users — the students Here we present a simple system made with the aim of illustrating the functioning of the microprocessor.

As a central processing unit (CPU) the Z—80 microprocessor has been used, one of the most widespread and performant of the day Its inner architecture (Fig. 1) as well as its functional features (soft and hardware) have been dealt with in many books of which we note [1—6]. In the works [7, 8] are described some systems in didactic purposes, namely that of learning the functioning

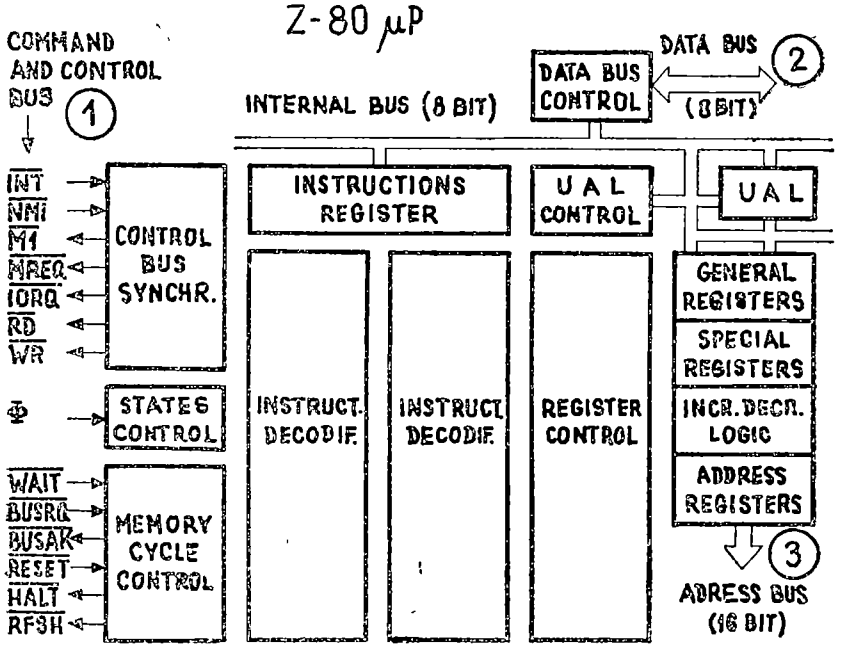

Fig 1

* *University of Cluj-Napoca, Department of Physics, 3400 Cluj-Napoca, Romania*

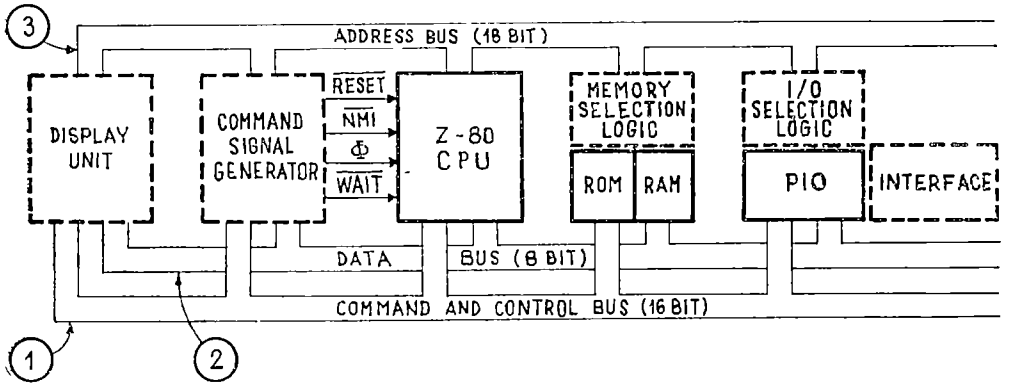

Fig 2

and usage of microprocessors, also made up with some other types of μP's. The possibilities of getting into interaction with Z—80 are marked in Fig. 1 with ① (control and command bus), ② (data bus) and ③ (address bus). Consequently we proposed and achieved the system in Fig 2 The commercialized component units are marked with solid lines, that is Z—80 CPU, ROM, RAM and PIO. With interrupted lines are delimited the functional units of own conception whose brief presentation is done in the following lines. Figure 3 shows the display unit on which by help of some 7-segment LEDs the contents

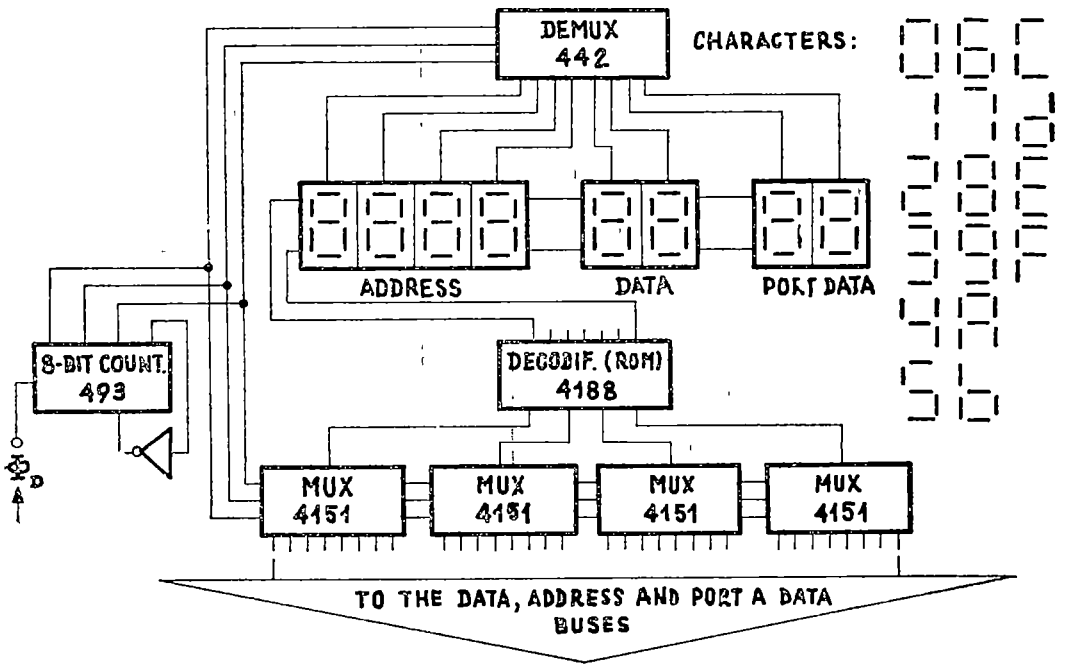

Fig 3

of address and data buses can be read together with the data at Port A access of the PIO The display is made in hexadecimal system (common in the μP technique) with the characters pointed on the right side of the illustration. The characters are formed by a ROM memory which supplies the missing seven-segment to four bit driver in hexadecimal code The activation of one of the lines of the command and control bus ($\overline{M1}$, $\overline{MREQ}$, $\overline{IORQ}$, $\overline{WR}$, $\overline{RD}$, $\overline{INT}$, $\overline{BUSRQ}$, $\overline{BUSAK}$, $\overline{HALT}$, $\overline{RFSH}$, $\overline{WAIT}$, $\overline{MS}$, $\overline{IOS}$, $\overline{COMP}$, $\overline{RESET}$ and $\overline{NMI}$) is put into evidence by the lightning of a LED drived by a logic inverter. The next unit, presented in Fig 4, is used in order to generate the command signals $\overline{RESET}$, $\overline{NMI}$, $\overline{WAIT}$ and the general clock signal Φ The switching of K_4 enables us to get over to a manual clock running, where the Φ pulses are generated by help of key K_1 The solution adopted for the clock generator takes into account the $Z-80$ μP feature of not permitting a longer period than $2\mu s$ for the zero level of the Φ pulse The TEST selector makes it possible to stop operation running at the appealing to some lines of command and control bus specified in the figure The STEP mode implies the waiting of the microprocessor at each machine-cycle, a state out of which it could be taken by the hand actioning of K_1 (In this case K_4 must have the automatic clock position). The K_3 switch serves to keep the processor in the WAIT state

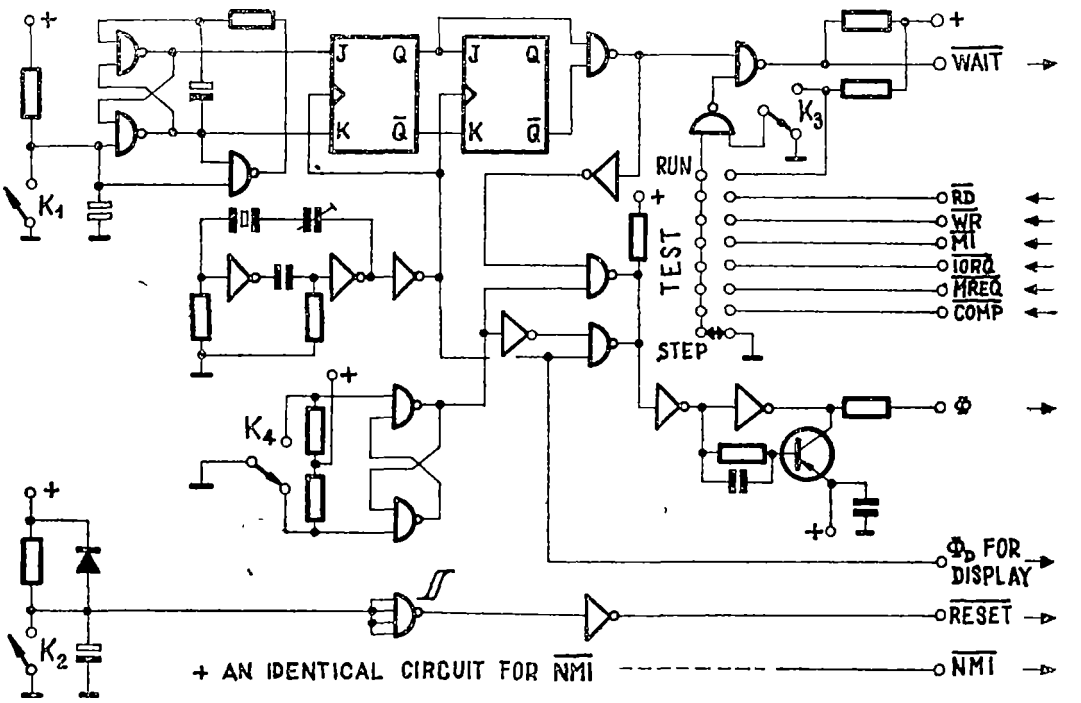

Fig 4

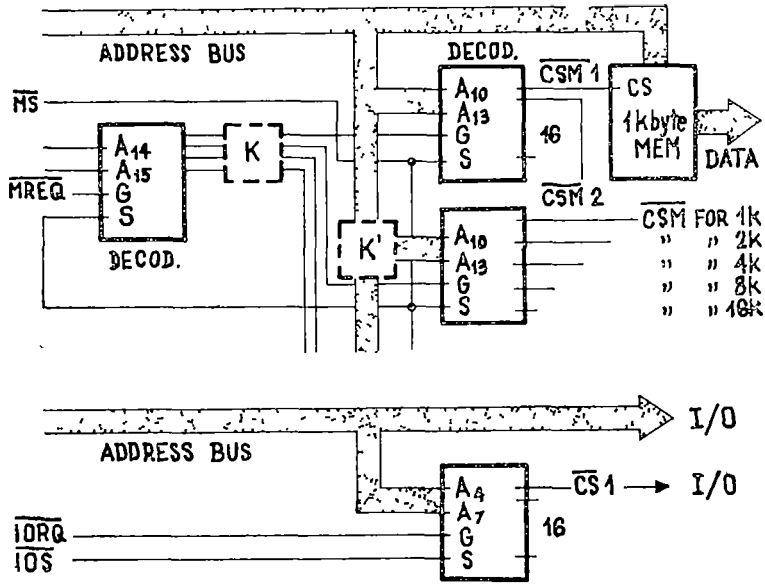

Fig 5

when the selection of the TEST mode is made By actioning K_2 the $\overline{RESET}$ line is activated, that is the initialization of the processor An identic circuit is employed to generate the $\overline{NMI}$ signal The circuit with transistor at the output of the clock generator serves for obtaining the pulse shape required by the producer Fig 5 gives both the memory selection and allocation circuit

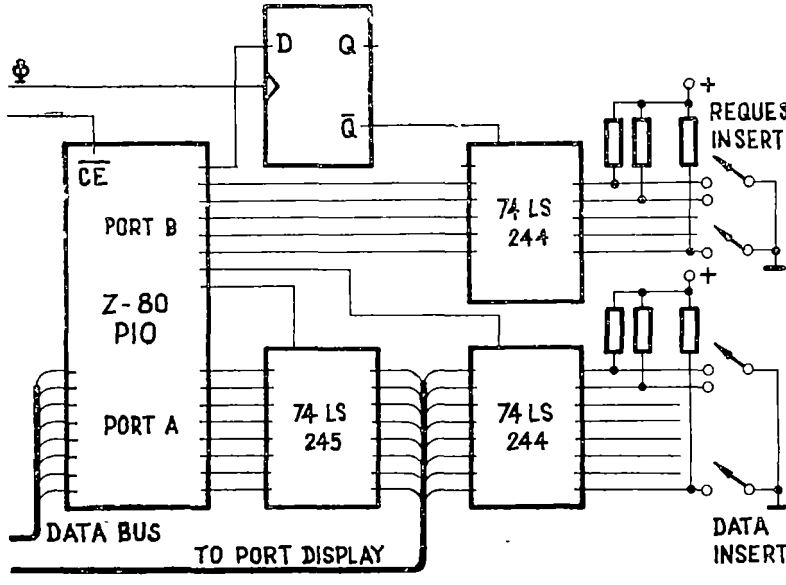

Fig 6

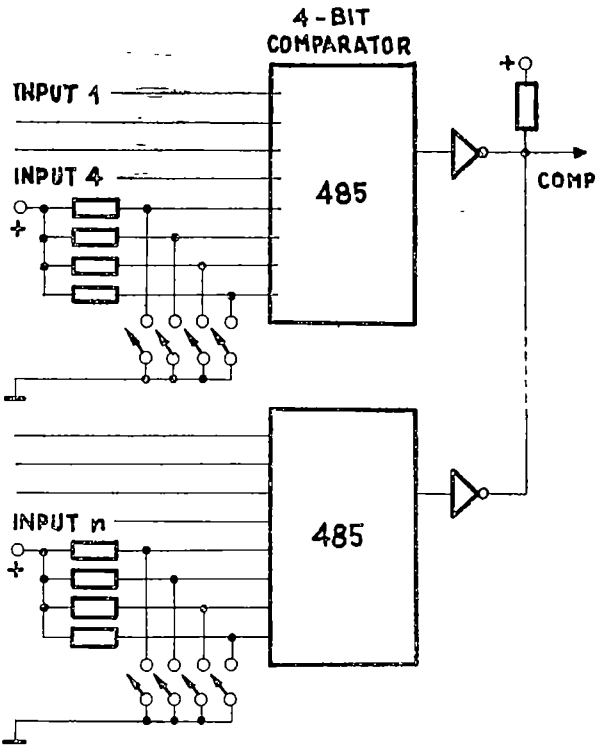

Fig 7

and the circuit for the selection of I/O chips The selection is thus organized that it should permit the usage of the whole assembly as a developing system. By help of the K switch, inaccessible from the front pannel, the MONITOR programm contained in ROM can be allocated in any zone of the memory. The K' switch is meant to match the selection in the case of some different memory capacities (1 — 16 kbyte) In Fig 6 we show a modality of achieving an interface adapted to the pursued purpose It allows for introduction of data and instructions in the memories and in the system by the two ports of the PIO The access through the interface is software-commanded by the MONITOR programm At last, Fig 7 exhibits the scheme of a circuit attended to the debugging of the hardware programmes

It must be mentioned the use in the presented system of the low-power Schottky TTL, in order to avoid overloading of basic circuitry The achieved implementation enables the system to be interconnected to other μP systems.

REFERENCES

1 Shima, M, „Z—80 Chip Set Herald Third μP Generation", Electronics, 19 August 1976
2. Lupu, C, Tepelea, V., Purice E, „Microprocesoare Aplicații", Ed Militară, București, 1982

3. Capatına, O., Cornea-Hasegan, M., Pusca, M, „Proiectarea cu microprocesoare", Ed Dacia, Cluj-Napoca, 1983
4. Vancsó, Gy, „Mikroszámítógép elemek a tervezéshez", Muszaki Kiadó, Budapest, 1984
5. Krizsán, Gy, „ZILOG-mikroprocesszor családok", LSI ATSZ — OMIKK, Budapest, 1984
6. Toacse, Gh, „Introducere în microprocesoare", Ed. Ştiinţifică şi Enciclopedică, Bucureşti, 1986
7. Coffran, J W., „Practical Troubleshooting Techniques for Microprocessor System", Prentice-Hall Inc, N. Jersey, 1981
8. Spanulescu I, Spanulescu S. I, „Prelucrarea, înregistrarea, transmiterea şi afişarea datelor Lucrări practice de laborator", Editată pentru uz intern, Universitatea din Bucureşti, 1984

CRONICĂ

A special meeting of the **PHYSICS DEPARTMENT,** held on December 19, 1986, was devoted to the presentation of the recent results obtained by the members of the department

S Codreanu, Some observations on chaos in non-linear systems,
T Beu and M Vasiu, Distribution of the impurities in plasma physics,
T Beu, The integral equation method for the inelastic scattering problem,
M. Crişan, Statistical theory of the clusters occurence in the short range spin glasses. critical behaviour, fractals,
Al Nicula, Spin image;
I Barbur and M. Crişan, Incommensurate structures and solitons in the ferroelectric phase transitions;
I Pop and C Hagan, The magnetic behaviour of the compounds $Tb_2Al_{17-x}Ni_x$,
V Crişan, A Vernes and C. Gorbea, Resonant states for transition metals from the iron group;
S Simon and Al Nicula, The study of the vitroceramics containing Europium by magnetic resonance,
L Cociu, M Peteanu and Al. Nicula, The kinetics of the anihilation of the paramagnetic defects in silicon doped by nuclear transition;
V Ioncu, G Cristea and E Tătaru, Generator for the linear recording of the spectra;
D Iancu, Microwaves oscillator in the X band with IMPATT diode accorded with VARACTOR diode;
F Puskas, S Selinger and F. F Puskas, Electronic device for the measurement in impulse regime of the electric resistivity of the semiconductors;
P Cioară, Manometric membrane of silicon germanium,
D G Popescu and G Varga, Microprocessor device for educational purposes;
G Cristea, NMR applications in medical research,
C Cosma, Environement radioactivity in the last period,
T. Iliescu, Data on interactions and molecular dynamics obtained from the profiles of the Raman spectra;
F Koch and S Koch, The use of pocket computers for the simmulation of the radioactive processes;
V. Cristea, E Trif, Al. Nicula, N. Iuga and P. Stetiu, Electrical properties of the Y sinthetic zeolites

ÎNTREPRINDEREA POLIGRAFICĂ CLUJ,
Municipiul Cluj-Napoca, Cd nr 547/1986

Revista științifică a Universității din Cluj-Napoca, **STUDIA UNIVERSITATIS BABEȘ-BOLYAI,** apare începînd cu anul 1986 în următoarele condiții:

matematică — trimestrial
fizică — semestrial
chimie — semestrial
geologie-geografie — semestrial pentru geologie și anual pentru geografie
biologie — semestrial
filosofie — semestrial
științe economice — semestrial
științe juridice — semestrial
istorie — semestrial
filologie — semestrial

STUDIA UNIVERSITATIS BABEȘ-BOLYAI, the scientific journal of the University of Cluj-Napoca, starting with 1986 is issued as follows

mathematics: quarterly
physics: biannually
chemistry: biannually
geology-geography: biannualy on geology and yearly on geography
biology: biannually
philosophy: biannually
economic sciences: biannually
juridical sciences: biannually
history: biannually
philology: biannually

43 904

Abonamentele se fac la oficiile poştale, prin factorii poştali şi prin difuzorii de presă, iar pentru străinătate prin „ROMPRESFILATELIA", sec orul export-import presă, P. O. Box 12—201, telex. 10376 prsfir, Bucureşti, Calea Griviţei nr. 64—66

Lei 35